Conversion of antigen-specific effector/memory T cells into Foxp3-expressing Treg cells by inhibition of CDK8/19

Masahiko Akamatsu[1,4†], Norihisa Mikami[2,3†], Naganari Ohkura[2,6], Ryoji Kawakami[2], Yohko Kitagawa[2], Atsushi Sugimoto[2], Keiji Hirota[3], Naoto Nakamura[4], Satoru Ujihara[4], Toshio Kurosaki[4], Hisao Hamaguchi[4], Hironori Harada[4], Guliang Xia[5], Yoshiaki Morita[1,4], Ichiro Aramori[1,4], Shuh Narumiya[1]*, Shimon Sakaguchi[2,3]*

[1]Center for Innovation in Immunoregulation Technology and Therapeutics, Kyoto University Graduate School of Medicine, Konoe-cho Yoshida, Sakyo-ku, Kyoto, Kyoto 606-8501, Japan

[2]Department of Experimental Immunology, WPI Immunology Frontier Research Center, Osaka University, Yamadaoka, Suita, Osaka 565-0871, Japan

[3]Department of Experimental Pathology, Institute for Frontier Medical Sciences, Kyoto University, 53 Kawahara-cho, Shogoin, Sakyo-ku, Kyoto, Kyoto 606-8507, Japan

[4]Drug Discovery Research, Astellas Pharma Inc., Miyukigaoka, Tsukuba, Ibaraki 305-8585, Japan

[5]Astellas Research Institute of America, Skokie, Illinois 60077, USA

[6]Department of Frontier Research in Tumor Immunology, Center of Medical Innovation and Translational Research, Graduate School of Medicine, Osaka University, Suita, Osaka 565-0871, Japan.

†These authors contributed equally to this work.

*Correspondence to:

Prof. Shuh Narumiya, e-mail: snaru@mfour.med.kyoto-u.ac.jp

Prof. Shimon Sakaguchi, e-mail: shimon@ifrec.osaka-u.ac.jp

Short title: Pharmacological generation of Treg cells

Abstract

A promising way to harness hazardous immune responses, such as autoimmune disease and allergy, is to convert disease-mediating T cells into immuno-suppressive regulatory T (Treg) cells. Here we show that chemical inhibition of cyclin-dependent kinases (CDK) 8/19, or knockdown/knockout of the CDK8 or CDK19 gene, is able to induce Foxp3, a key transcription factor controlling Treg cell function, in antigen-stimulated effector/memory as well as naïve $CD4^+$ and $CD8^+$ T cells. The induction was associated with STAT5 activation, independent of TGF-β action, and not affected by inflammatory cytokines. Furthermore, *in vivo* administration of a newly developed CDK8/19 inhibitor along with antigen immunization generated functionally stable antigen-specific $Foxp3^+$ Treg cells, which effectively suppressed skin contact hypersensitivity and autoimmune disease in animal models. The results indicate that CDK8/19 is physiologically repressing Foxp3 expression in activated conventional T cells and that its pharmacological inhibition enables conversion of antigen-specific effector/memory T cells into $Foxp3^+$ Treg cells for the treatment of various immunological diseases.

One Sentence Summary:

Chemical inhibition of CDK8/19 can convert naïve and memory/effector T cells into regulatory T cells capable of treating immunological diseases.

Introduction

Naturally occurring $CD4^+$ regulatory T (Treg) cells expressing the transcription factor forkhead box protein 3 (Foxp3) are essential for the maintenance of immunological self-tolerance and homeostasis (1). Anomalies of $Foxp3^+$ natural Treg (nTreg) cells in number or function, for example, due to mutations of the Foxp3 gene cause various immunological diseases including autoimmune disease, allergy, and inflammatory bowel disease (1, 2). Moreover, increasing the number of $Foxp3^+$ nTreg cells or augmenting their suppressive function is able to treat immunological diseases and control graft rejection in organ transplantation (1). While the majority of nTreg cells are produced by the thymus as a functionally distinct and mature T cell population (tTreg cells), conventional T (T conv) cells in the periphery can acquire similar Treg phenotype and function (peripherally induced Treg [pTreg] cells), for example, in response to a particular species of commensal bacteria in the intestine (3). With these findings on physiological generation of $Foxp3^+$ Treg cells in the thymus and the periphery, it is an ideal way for antigen-specific immune suppression to develop methods for converting antigen-specific Tconv cells, especially effector or memory T cells mediating harmful immune responses, into functionally stable Foxp3-expressing Treg cells *in vivo* and *in vitro*.

It has been well established that *in vitro* antigenic stimulation in the presence of TGF-β is able to elicit Foxp3 expression in Tconv cells (4, 5). This *in vitro* TGF-β-dependent generation of induced Treg (iTreg) cells is, however, only attainable from naïve Tconv cells, not from effector or memory T cells, and hindered by the presence of pro-inflammatory cytokines (4, 5). In addition, TGF-β-induced iTreg cells are unstable in sustaining *in vivo* suppressive function mainly because of their failure to acquire stable Treg-specific epigenomic changes in Foxp3 and other Treg signature genes, which limits their therapeutic application (5-7). These findings prompted us to search for chemical compounds that can convert not only naïve but also effector or memory Tconv cells into functionally stable, antigen-specific $Foxp3^+$ Treg cells in a TGF-β-independent manner even in the presence of pro-inflammatory cytokines.

Here we show that, by screening chemical compounds for *in vitro* activity to generate $Foxp3^+$ T cells from Tconv cells, pharmacological inhibition of CDK8 and its paralogue CDK19, which are reversibly associated with the Mediator complex and mainly controlling the function of transcription factors positively and negatively (8), is able to induce Foxp3 not only in naïve T cells but also in effector/memory type T cells. The converted Treg cells are capable of suppressing autoimmune and allergic immune responses in animal models. Our

results indicate that the CDK8/CDK19 signaling is physiologically repressing Foxp3 expression in activated Tconv cells and that the inhibition of the signaling is sufficient to induce Foxp3 in activated and differentiated Tconv cells, converting them into antigen-specific Treg-like suppressive T cells clinically applicable. These findings would also facilitate our understanding of physiological mechanisms of pTreg cell generation and peripheral immune tolerance.

Results

Induction of Foxp3 expression in effector/memory T cells as well as naïve T cells by a chemical compound.

We first screened our chemical library composed of ~5000 structurally different small molecules for the compounds capable of generating Foxp3$^+$ Treg cells from Tconv cells upon *in vitro* polyclonal TCR stimulation. When mouse Tconv cells were stimulated *in vitro* with anti-CD3 and anti-CD28 mAb-coated beads in the presence of IL-2, the compound AS2863619 (4-[1-(2-methyl-1*H*-benzimidazol-5-yl)-1*H*-imidazo[4,5-*c*]pyridin-2-yl]-1,2,5-oxadiazol-3-amine dihydrochloride) (**Fig. 1A**), abbreviated as AS hereafter, was found to possess the activity to generate Foxp3$^+$ T cells from naive Foxp3$^-$CD4$^+$ Tconv cells in a dose-dependent fashion (**fig. S1A**). It did not exhibit cellular toxicity or hinder proliferative activity of Tconv cells in the concentration range possessing Foxp3-inducing activity (**fig. S1A**). Similar AS treatment induced Foxp3 in CD8$^+$ Tconv cells as well (**Fig. 1B**). It also significantly enhanced FOXP3 expression in human CD4$^+$ and CD8$^+$ Tconv cells in the peripheral blood, although TCR stimulation per se elicited the expression at a low level (9, 10) (**fig. S2**).

Notably, AS induced Foxp3 in phenotypically effector/memory (CD44^{high}CD62L^{low}) CD4$^+$ Tconv cells as well as naive (CD44^{low}CD62L^{high}) Foxp3$^-$CD4$^+$ Tconv cells (**Fig. 1B**). A combination of AS and TGF-β synergistically induced Foxp3 in both naïve and effector/memory populations, while TGF-β alone generated Foxp3$^+$ cells only from naive Tconv cells.

Unlike other reported Foxp3-inducing substances, such as retinoic acid (**fig. S1B**), which require exogenous TGF-β for iTreg cell induction (11-13), TGF-β neutralization (**Fig. 1B**) or a serum-free condition (**fig. S1C**) did not affect the AS-dependent *in vitro* Foxp3 induction. IL-2 neutralization or IL-2 addition dampened or enhanced, respectively, the induction, indicating requirement of IL-2 for the AS generation of Foxp3$^+$ T cells (**fig. S1D**).

Furthermore, a Th1-, Th2-, Th17, or Th9-inducing condition containing inflammatory cytokines such as IFN-γ, IL-4, and IL-6, which inhibited TGF-β-dependent Foxp3 induction (14, 15), did not hamper the AS-dependent Foxp3 induction in $CD4^+$ Tconv cells (**Fig. 1C** and **D**).

With $CD4^+$ Tconv cells from DO11.10 transgenic mice expressing an ovalbumin (OVA) peptide-specific transgenic TCR (which can be detected by the clonotype-specific KJ1-26 mAb, ref.16), the compound induced Foxp3 expression in OVA-stimulated KJ1-26^+ T cells but not in non-stimulated KJ1-26^- T cells (**Fig. 1E** and **F**), indicating the requirement of antigenic stimulation for the AS-dependent $Foxp3^+$ cell generation.

Although TGF-β was not required for the induction, AS-induced iTreg cells were similar to TGF-β-induced ones in the expression of Treg function-associated cell surface molecules, such as CD25, CTLA-4 and GITR (**Fig. 1G)**, in the activity of *in vitro* suppression (**Fig. 1H**), and in non-possession of Treg-specific DNA hypomethylation (17) (**fig. S3**). The compound scarcely affected nTreg function and proliferation *in vitro* (**fig. S4**).

RNA-seq analysis of AS-treated or non-treated $CD4^+$ Tconv, B, or dendritic cells (DCs) revealed differentially expressed genes (DEGs) in each population: the compound up-regulated the transcription of a limited number (~20) of genes, including Foxp3, in $CD4^+$ Tconv cells, without up-regulation of these genes in B or DCs (**fig. S5**). There was no increase in the transcription of immunosuppressive molecules such as TGF-β, IL-10, IL-35, and IDO by AS-treated T, B, and DCs (data not shown).

These results taken together indicate that AS is able to directly, without antigen-presenting cells (APCs), induce Foxp3 *in vitro* not only in naive Tconv cells but also in antigen-activated or effector/memory Tconv cells even in the presence of various inflammatory cytokines. The induction is TGF-β–independent, IL-2-dependent, and requires TCR stimulation, thus enabling conversion of antigen-specific Tconv cells into $Foxp3^+$ suppressive T cells without TGF-β.

CDK8/19 as a target of Foxp3-inducing AS.

In order to determine the target molecule(s) of AS in its Foxp3 induction, we conducted affinity purification (18) of AS-bound proteins by conjugating AS3309191, an active AS analogue, with photoreactive affinity capture linker and mixing the conjugate with the lysates of mouse EL4 T cell lymphoma cells in the presence or absence of an excess amount of AS analogs (**fig. S6A, S6B**). This affinity purification followed by mass

spectrometry analysis identified CDK8, CDK19, GSK3α and GSK3β as candidate AS-binding proteins (**Fig. 2A**). We therefore assessed several compounds, including AS, two AS analogs (AS3334366 and AS3196162, **fig. S6C**), a CDK8/19 inhibitor [senexin A (19)], and a GSK3α/β inhibitor [CHIR99021 (20)], for their activity to inhibit these kinases and thereby induce Foxp3 in $CD4^+$ Tconv cells (**Fig. 2B**). The Foxp3-inducing potency of these compounds correlated well with their inhibitory activities on CDK8 and CDK19 but not on the GSK3 isoforms. In addition, in a kinase selectivity-profiling assay for evaluating 189 other kinases, none were inhibited by AS more than half of control (**Table. S1**). Thus, CDK8 and CDK19 are most likely the target molecules of AS in its Foxp3 induction.

The expression of CDK8 was low in naïve $CD4^+$ Tconv cells and increased within 24 hours after *in vitro* TCR stimulation, while CDK19 and cyclin C, another component of the CDK8 kinase module, was constitutively expressed before and after stimulation (**Fig. 2C**), suggesting that CDK8, either alone or together with CDK19, might be repressing Foxp3 expression in activated Tconv cells. To assess this possibility, we depleted CDK8 and CDK19 in $CD4^+$ Tconv cells by RNA interference (RNAi) and found a significant increase of Foxp3 transcription not only in CDK8-depleted cells but also in CDK19-depleted cells upon TCR stimulation (**Fig. 2D**). In addition, retroviral overexpression of the kinase-dead (KD) mutants, D173A CDK8 and D173A CDK19, which possessed dominant-negative effects on wild-type (WT) CDK8/19 (**fig. S7A**), generated $Foxp3^+$ cells from $CD4^+$ Tconv cells even in the absence of TGF-β or in the presence of IL-6, while overexpression of WT CDK8 or CDK19 did not (**Fig. 2E, fig. S7B**). Luciferase reporter assays harboring the Foxp3 promoter sequence also showed that AS enhanced Foxp3 transcriptional activity in WT, CDK8- or CDK19-deficient EL4 cells, but not in CDK8/19 double-deficient EL4 cells (**Fig 2F, fig. S8**). The latter were still responsive to TGF-β-dependent Foxp3 induction in luciferase assay with a SMAD3-responsive Foxp3 CNS1-containing construct (**fig. S8**).

Next, to examine whether CDK8 dysfunction in primary Tconv cells could induce Foxp3 expression upon *in vivo* antigenic stimulation, we retrovirally overexpressed the KD mutant of CDK8, together with the LNGFR reporter, in DO11.10 TCR^+CD4^+ T cells and transferred them into T cell-deficient BALB/c nude (nu/nu) mice, expanded the transferred T cells in an antigen-nonspecific manner by administration of one dose of IL-2/anti-IL-2 complex, and then immunized the mice with OVA (**Fig. 2G** and **H**, **fig. S9**). The transferred $CD4^+$ T cells expressing the KD mutant CDK8 gave rise to $Foxp3^+$ T cells following OVA immunization, whereas those overexpressed with WT CDK8 did not.

These *in vitro* and *in vivo* results collectively indicate that AS is able to elicit transcription of the Foxp3 gene in activated Tconv cells by inhibiting the kinase activity of CDK8/19, which appears to physiologically repress Foxp3 expression in activated Tconv cells.

Interaction of CDK8/19 with STAT5 in Foxp3 induction.

The following findings suggested possible involvement of STAT5 in the CDK8/19 inhibition-dependent Foxp3 induction: CDK8 phosphorylates the serine residue in the PSP (Pro-Ser-Pro) motif of the STAT proteins including STAT5 (21); AS and IL-2, whose signaling requires STAT5, synergistically enhanced $Foxp3^+$ T cell generation (**fig. S1D**); in addition, constitutive activation of STAT5 is able to induce Foxp3 expression in Tconv cells (22, 23). We therefore examined possible effects of AS on the phosphorylation of STAT5 in inducing Foxp3 in Tconv cells. Immunoprecipitation with anti-CDK8 indeed co-precipitated STAT5b, together with MED12, a component of the CDK8 kinase module of the Mediator complex, from activated $CD4^+$ Tconv cells and more strongly from those retrovirally overexpressing both CDK8 and STAT5b (**Fig. 3A**). Incubation of recombinant WT CDK8 with recombinant STAT5b resulted in phosphorylation of the serine residue of the latter whereas incubation of KD CDK8 with STAT5b did not; further, AS inhibited the STAT5b serine phosphorylation by WT CDK8 (**Fig. 3B**). In addition, anti-CD3/anti-CD28 mAb stimulation induced phosphorylation of both serine and tyrosine residues of STAT5 in $CD4^+$ T cells; and AS suppressed serine phosphorylation of the PSP motif of STAT5b to ~40%, while enhancing tyrosine phosphorylation in the C-terminal domain to ~160% of control-treated samples (**Fig. 3C**). The AS inhibition of STAT5b-serine phosphorylation was indeed correlated with Foxp3 induction in a dose-dependent manner (**fig. S10**). In addition, CDK8 and STAT5 formed endogenous complexes in activated $CD4^+$ Tconv cells as indicated by their co-localization shown by proximity ligation assay (PLA) (**Fig. 3D** and **3E**) and as co-staining by anti-CDK8 and anti-STAT5 antibodies (**Fig. 3F**). Furthermore, overexpression of S730A-STAT5b, a serine-phosphorylation-resistant STAT5b mutant capable of increasing the tyrosine phosphorylation (24, 25), in $CD4^+$ T cells generated $Foxp3^+$ T cells more efficiently than WT-STAT5 overexpression; and AS augmented the WT-STAT5-induced generation to an equivalent level as attained by the mutant (**Fig. 3G**). It was also noted in these experiments that AS treatment of S730A-STAT5b overexpressing cells significantly increased $Foxp3^+$ T cells, suggesting a possible involvement of a signaling pathway other than the STAT5-mediated one in the Foxp3 induction by CDK8/19 inhibition. It is thus likely

as a possible, but not a sole mechanism that AS inhibits activated CDK8/19 to phosphorylate the serine residue in the PSP motif of STAT5; the diminished serine phosphorylation augments the retention of the tyrosine phosphorylated STAT5 in the nucleus, leading to enhanced activation of STAT5, which consequently activates the Foxp3 gene.

Genome-wide enhancement of STAT5 binding by AS.

To determine then whether AS augmented STAT5 binding in the genome, we conducted whole-genome chromatin IP sequencing (ChIP-seq) of AS-treated activated Tconv cells. At the Foxp3 gene locus, AS enhanced STAT5 binding to the Foxp3 CNS0 region, which is the enhancer region first activated in thymic Treg cell development (26), and, to a lesser extent, to the Foxp3 promoter and the CNS2 region, a critical enhancer site for Foxp3 transcription (27) (**Fig. 4A**). ChIP-qPCR with anti-STAT5 or anti-pSTAT5 confirmed STAT5 and pSTAT5 binding to these regions, especially to the CNS0 region (**Fig. 4B**). CDK8 also bound to the CNS0 and the promoter regions in AS-treated activated Tconv cells (**fig. S11**). The CNS0 enhancer region in AS-treated or non-treated Tconv cell equally possessed activated H3K27ac as assessed by H3K27ac-ChIP-seq and was in an open chromatin state by ATAC-seq (**Fig. 4A**). The STAT5 ChIP-seq also revealed globally increased STAT5 binding at activated enhancer regions, marked by H3K4me1 or H3K27ac modifications (**Fig. 4C**). When STAT5 binding peaks were separated into two groups, one unchanged (5353 peaks) or the other (876 peaks) augmented by AS treatment, the latter located mainly in intron and intergenic regions, whereas the former mainly in promoter regions (**Fig. 4D**). Expression of STAT5-associated genes with STAT5 binding in enhancers was up-regulated highly significantly by AS treatment, whereas expression of those with STAT5 binding in promoters were not (**Fig. 4E**). The former genes up-regulated by AS in Tconv cells included various Treg function-associated genes (e.g., *Foxp3*, *Il2ra*, *Tnfrsf18*, *Foxo1*, *Ccr4*, *Icos*). These STAT5 ChIP-seq analyses also revealed little direct histone modification by AS itself (**fig. S11**). Taken together, STAT5 activation enhanced by AS inhibition of CDK8/19 and consequent transcription of STAT5-bound genes including *Foxp3* is a key mechanism of AS-induced Foxp3 expression in activated Tconv cells.

AS-induced *in vivo* Foxp3 induction in antigen-activated T cells.

To determine then whether AS was able to induce Foxp3 *in vivo* in Tconv cells in an antigen-specific manner, we orally administered AS to DO11.10 TCR transgenic mice on the RAG2-deficient background, which harbored no thymus-derived Treg cells (1), and

immunized the mice with OVA during AS treatment (**Fig. 5A**). The treatment with 30 mg/kg dose, which attained a serum concentration equivalent to an *in vitro* Foxp3-inducing dose without discernible *in vivo* toxicity (**fig. S12**) (28), induced Foxp3 in KJ1-26$^+$ T cells, while AS administration alone did not. Similarly in RAG2-sufficient DO11.10 mice, OVA immunization and following AS-treatment specifically generated KJ1.26$^+$ Foxp3$^+$ T cells, with concurrent antigen-specific suppression of the activation of KJ1.26$^+$ but not KJ1.26$^-$ Foxp3$^-$ Tconv cells (**fig. S13**).

RNA-seq analysis of the AS-induced pTreg cells in RAG2-deficient DO11.10 TCR transgenic mice revealed their gene expression pattern to be more similar to nTreg cells, especially activated nTreg cells, compared with AS-treated or non-treated Foxp3$^-$ Tconv cells (**Fig. 5B** and **fig. S14**). The analysis also depicted *Klrg1* as being highly expressed in AS-induced pTreg cells but not in nTreg cells or Tconv cells after antigen immunization (**fig. S14**). Flow cytometric analysis of AS-induced pTreg cells showed an expression pattern of Treg signature molecules with a slightly less activated profile (i.e., slightly lower expression of CD25, GITR, and CTLA-4) and with lower Neuropilin 1 (NRP1) and negative expression of integrin β8, both profiles being indicative of pTreg cells (7, 29-31) (**Fig. 5C**). Consistent with the gene expression profile, a population of AS-induced pTreg cells showed high expression of the KLRG1 protein, a possible marker for terminally differentiated Treg cells (32). Moreover, Treg-specific DNA demethylation status, assessed by bisulfite sequencing (17, 33), revealed that, unlike *in vitro* AS-induced Foxp3$^+$ cells, the i*n vivo* AS-induced pTreg cells possessed stable Treg-specific demethylation at the Foxp3 and Helios gene loci (**Fig. 5D**). These pTreg cells also exhibited suppressive activity as potently as nTreg cells (**Fig. 5E**). In addition, injection of IL-2/anti-IL-2 mAb complexes augmented *in vivo* AS-dependent KLRG1$^+$ pTreg cell induction after OVA immunization in RAG-deficient DO11.10 mice (**fig. S15)**.

Thus, with antigenic stimulation, AS is able to generate *in vivo* from Tconv cells antigen-specific, functionally stable, and highly differentiated Foxp3$^+$ pTreg cells.

Therapeutic effects of AS on allergy and autoimmunity in animal models.

The above results prompted us to assess *in vivo* therapeutic effects of AS in several disease models. In a skin contact hypersensitivity model, AS treatment after sensitization with DNFB dampened the degree of the secondary response, with milder infiltration of inflammatory cells into the skin and decreased ratios of IFN-γ$^+$ cells in the regional lymph nodes when compared with vehicle-treated control mice (**Fig. 6A-D**). Treg depletion before

the elicitation of the secondary response abolished AS-induced suppression. Notably, KLRG1^{+}Foxp3^{+} T cells were specifically increased in DNFB-sensitized AS-treated mice (**Fig. 6E**). An increase of whole Foxp3^{+} cells, mainly KLRG1^{-}Foxp3^{+} cells, was also noticed in non-immunized AS-treated mice, suggesting that AS might have converted some self-reactive Tconv cells into Foxp3^{+} cells or transiently expanded self-reactive nTreg cells via activating DCs presenting self-antigens (**fig. S16**). AS treatment also suppressed delayed type hypersensitivity against OVA in normal mice, with an increase of KLRG1^{+} Foxp3^{+} T cells in draining lymph nodes, contrasting with dexamethasone as a control, which exhibited non-specific suppression of effector T cells without increasing Treg cells (**fig. S17**). In addition, in NOD mice, which spontaneously developed histologically evident insulitis by 8 weeks of age in our mouse facility, AS treatment from 8 weeks of age significantly reduced the incidence of clinically evident diabetes (**Fig. 6F**), with much milder insulitis development (**Fig. 6G**), significantly higher ratios of KLRG1^{+}Foxp3^{+} T cells (**Fig. 6H**), and smaller ratios of Th1 cells in the regional lymph nodes (**Fig. 6H**). Similar AS treatment also suppressed mouse experimental allergic encephalomyelitis with a significant increase of KLRG1^{+}Foxp3^{+} T cells and a decrease of Th17 cells in the regional lymph nodes (**Fig. 6I** and **6J**). These results collectively indicate that AS is able to control acute and chronic, physiological and pathological immune responses, including allergy and autoimmunity, by generating antigen-specific pTreg cells.

Discussion

A key feature of Foxp3 induction in Tconv cells by pharmacological inhibition of CDK8/19, or knock-down/knock-out of the CDK8 or CDK19 gene, is that it does not require exogenous TGF-β, as illustrated by the *in vitro* Foxp3 induction under TGF-β neutralization and in an APC-free or a serum-free condition. The CDK8/19 inhibitor AS is therefore distinct from other Foxp3 inducing substances such as rapamycin, retinoic acid and butyrate (11-13), which all require TGF-β for initial Foxp3 induction. In addition, unlike TGF-β-induced iTreg cells, AS-induced iTreg cells can be induced in the presence of inflammatory cytokines such as IL-4, IL-1L6, and IFN-γ, which appear to hamper Foxp3 gene activation via activation of STATs (34). Unlike TGF-β, AS is able to generate iTreg cells not only from naïve Tconv cells but also effector/memory Tconv cells. Furthermore, AS cannot induce Foxp3 in CDK8 and CDK19 double-deficient T cells, whereas TGF-β can. Yet there are also common properties between the TGF-β- and AS-induced iTreg cells; for example, both require TCR

and IL-2 stimulation for their generation and both are devoid of Treg-type DNA hypomethylation, which is present in nTreg cells and required for stable Treg function (17). These distinct or common immunological properties, together with a synergism of AS and TGF-β in Foxp3 induction, suggest that CDK8/19-dependent signaling pathway and TGF-β-dependent one are distinct but converge on the activation of Foxp3 gene, as discussed below.

CDK8 and its paralogue CDK19, which assemble with Cyclin C, Med12 and Med13 to form the kinase module, are reversibly associated with the Mediator complex, controlling gene transcription positively and negatively (35). Although CDK8 and CDK19 are reported to be mutually exclusive in the association with the kinase module, knockdown or knockout of either CDK8 or CDK19, or the expression of a kinase-dead form of either one, was sufficient to induce Foxp3 expression in primary Tconv cells. This finding suggests that CDK8 and CDK19 are not mutually compensatory or redundant in Foxp3 induction in Tconv cells. CDK8 has been implicated in the regulation of cytokine signaling, for example, via controlling STATs (21, 36). Although CDK8 has been shown to be involved in oncogenic pathways such as the Wnt–β-catenin, p53, NF-κB, microRNA, or TGF-β pathways (37-39), inhibitors of NF-κB, GSK3, or other pathways failed to hamper *in vitro* AS-mediated Foxp3 induction (**fig. S18**). It is required to determine how each CDK8 inhibitor affects the structure and function of CDK8 and consequently modulates distinct signaling pathways to further understand the role of CDK8/19 in Foxp3 induction.

AS-inhibited CDK8/19 suppresses the serine phosphorylation in the PSP motif of STAT5 and somehow augments phosphorylation of the tyrosine residue in the C-terminal domain, leading to enhanced activation of STAT5 and consequently the activation of STAT5-bound various genes including Treg signature genes such as *Foxp3* and *Cd25*. At the Foxp3 gene locus, pSTAT5 strongly binds to the CNS0 region and to a lesser extent to the promoter and the CNS2 region. We have previously shown that CNS0 is an enhancer region first and profoundly activated in the differentiation of tTreg cells in the thymus, and also slightly activated (e.g., H3K27ac modified) in Tconv cells from their thymic $CD4^+CD8^+$ stage on, but not in other immune cell lineages such as B cells and DCs (24). This T cell-specific role of the CNS0 enhancer region and STAT5 binding to the region might contribute to T cell-specific expression of Foxp3 by AS. Taken together, these findings suggest that, in TCR stimulated Tconv cells expressing the IL-2 receptor, CDK8/19 activated by TCR signal physiologically suppresses IL-2-dependent STAT5 activation, thus attenuating STAT5-dependent gene activation to a certain extent and thereby suppressing Foxp3 expression (**fig.**

S19). The balance between the TCR-CDK8/19-STAT5 signaling pathway inhibiting Foxp3 expression and the IL-2R-STAT5 pathway inducing Foxp3 expression might be altered transiently in Tconv cells upon TCR stimulation, resulting in transient and low-level Foxp3 expression in activated human Tconv cells without exhibiting suppressive activity or acquiring Treg-specific epigenetic changes (10, 40).

In contrast with *in vitro* AS or TGF-β-induced iTreg cells, which were devoid of Treg-specific hypomethylation in Treg signature genes, *in vivo* AS-induced pTreg cells possessed stable Treg-specific demethylation at the Foxp3, Helios and other gene loci, and robust suppressive activity similar to activated nTreg cells. Their low expression of NRP1 and Integrin β8 indicates that they are similar to pTreg cells naturally induced from Tconv cells, for example, by homeostatic Tconv activation and differentiation in a T-lymphopenic environment (17). In addition, they characteristically express KLRG1, suggesting that they are in a highly activated or differentiated state with strong suppressive activity (32). These results collectively indicate that *in vivo* AS-induced $Foxp3^+$ T cells are able to gradually acquire Treg-specific epigenetic alterations, differentiating into functionally stable $Foxp3^+$ pTreg cells possessing a more nTreg-like gene expression profile. AS treatment for a limited period may thus enable establishing long-term immunosuppression by generating functionally stable pTreg cells. It remains to be determined what *in vivo* host-derived factors, which appear to be missing *in vitro*, are responsible for the epigenetic conversion of Tconv into Treg cells by *in vivo* AS treatment.

We have thus shown that pharmacological inhibition of CDK8/19, or knock-down or knock-out of the CDK8 or CDK19 gene, is sufficient to induce Foxp3 in activated Tconv cells by mainly, if not solely, modulating STAT5. A key therapeutic advantage of this AS-dependent generation of $Foxp3^+$ T cells is that effector/memory or antigen-primed T cells mediating a particular pathological (e.g., autoimmunity and allergy) or a physiological immune response (e.g., rejection of an organ transplant) can be converted into antigen-specific Treg cells even in a cytokine-abundant inflammatory environment. Further elucidation of the molecular basis of CDK8/19-STAT5 signal-dependent Foxp3 induction, in particular, in effector/memory Tconv cells, will facilitate our understanding of peripheral immune tolerance contributed by pTreg cells and enable devising novel therapies of immunological diseases by the use of $Foxp3^+$ Treg cells *de novo* pharmacologically generated *in vivo* and *in vitro*.

Supplementary Materials

Materials and Methods

Figures S1-S19

Tables S1-S2

References and Notes

1. S. Sakaguchi, T. Yamaguchi, T. Nomura, M. Ono, Regulatory T cells and immune tolerance. *Cell* **133**, 775-787 (2008).
2. A. Y. Rudensky, Regulatory T cells and Foxp3. *Immunol Rev* **241**, 260-268 (2011).
3. T. Tanoue, K. Atarashi K, K. Honda K, Development and maintenance of intestinal regulatory T cells. *Nat Rev Immunol* **16**, 295-309 (2016).
4. W. Chen, W. Jin, N Hardegen, K.J. Lei, L. Li, N. Marinos, G. McGrady, S.M. Wahl, Conversion of peripheral CD4+CD25- naive T cells to CD4+CD25+ regulatory T cells by TGF-beta induction of transcription factor Foxp3. *J Exp Med* **198**, 1875-1886 (2003).
5. L. Xu, A. Kitani, W. Strober, Molecular Mechanisms Regulating TGF-β-Induced Foxp3 Expression. *Mucosal Immunol* **3**, 230-238 (2010).
6. A. M. Bilate, J. J. Lafaille, Induced CD4+Foxp3+ regulatory T cells in immune tolerance. *Annu Rev Immunol* **30**, 733-758 (2012).
7. E. M. Shevach, A. M. Thornton, tTregs, pTregs, and iTregs: similarities and differences. *Immunol Rev* **259**, 88-102 (2014).
8. B.L. Allen, D.J. Taatjes, The Mediator complex: a central integrator of transcription. *Nat Rev Mol Cell Biol* **16**, 155-166 (2015).
9. M.R. Walker, D.J. Kasprowicz, V.H. Gersuk, A. Benard, M. Van Landeghen, J.H. Buckner, S.F. Ziegler, Induction of FoxP3 and acquisition of T regulatory activity by stimulated human CD4+CD25- T cells. *J Clin Invest* **112**, 1437-1443 (2003).
10. H. Yagi, T. Nomura, K. Nakamura, S. Yamazaki, T. Kitawaki, S. Hori, M. Maeda, M. Onodera, T. Uchiyama, S. Fujii, S. Sakaguchi, Crucial role of FOXP3 in the development and function of human CD25+CD4+ regulatory T cells. *Int Immunol* **16**, 1643-1656 (2004).
11. S. Jhunjhunwala, L.C. Chen, E.E. Nichols, A.W. Thomson, G. Raimondi, S.R. Little, All-trans retinoic acid and rapamycin synergize with transforming growth factor-β1 to

induce regulatory T cells but confer different migratory capacities. *J Leukoc Biol* **94**, 981-989 (2013).

12. Y. Furusawa, Y. Furusawa, Y. Obata, S. Fukuda, T.A. Endo, G. Nakato, D. Takahashi, Y. Nakanishi, C. Uetake, K. Kato, T. Kato, M. Takahashi, N.N. Fukuda, S. Murakami, E. Miyauchi, S. Hino, K. Atarashi, S. Onawa, Y. Fujimura, T. Lockett, J.M. Clarke, D.L. Topping, M. Tomita, S. Hori, O. Ohara, T. Morita, H. Koseki, J. Kikuchi, K. Honda, K. Hase, H. Ohno, Commensal microbe-derived butyrate induces the differentiation of colonic regulatory T cells. *Nature* **504**, 446-450 (2013).
13. D. Mucida, Y. Park, G. Kim, O. Turovskaya, I. Scott, M. Kronenberg, H. Cheroutre, Reciprocal TH17 and regulatory T cell differentiation mediated by retinoic acid. *Science* **317**, 256-260 (2007).
14. E. Bettelli, Y. Carrier, W. Gao, T. Korn, T.B. Strom, M. Oukka, H.L. Weiner, V.K. Kuchroo, Reciprocal developmental pathways for the generation of pathogenic effector TH17 and regulatory T cells. *Nature* **441**, 235-238 (2006).
15. J. Wei, O. Duramad, O.A. Perng, S.L. Reiner, Y.J. Liu, F.X. Qin, Antagonistic nature of T helper 1/2 developmental programs in opposing peripheral induction of Foxp3+ regulatory T cells. *Proc Natl Acad Sci U S A* **104**, 18169-18174 (2007).
16. K.M. Murphy, A.B. Heimberger, D.Y. Loh, Induction by antigen of intrathymic apoptosis of CD4+CD8+TCRlo thymocytes in vivo. *Science* **250**, 1720-1723 (1990).
17. N. Ohkura, M. Hamaguchi, H. Morikawa, K. Sugimura, A. Tanaka, Y. Ito, M. Osaki, Y. Tanaka, R. Yamashita, N. Nakano, J. Huehn, H.J. Fehling, T. Sparwasser, K. Nakai, S. Sakaguchi. T cell receptor stimulation-induced epigenetic changes and Foxp3 expression are independent and complementary events required for Treg cell development. *Immunity* **37**, 785-799 (2012).
18. M. Terajima, Y. Kaneko-Kobayashi, N. Nakamura, M. Yuri, M. Hiramoto, M. Naitou, K. Hattori, H. Yokota, H. Mizuhara, Y. Higashi, Inhibition of c-Rel DNA binding is critical for the anti-inflammatory effects of novel PIKfyve inhibitor. *Eur J Pharmacol* **780**, 93-105 (2016).
19. D. C. Porter, E. Farmaki, S. Altilia, G.P. Schools, D.K. West, M. Chen, B.D. Chang, A.T. Puzyrev, C.U. Lim, R. Rokow-Kittell, L.T. Friedhoff, A.G. Papavassiliou, S. Kalurupalle, G. Hurteau, J. Shi, P.S. Baran, B. Gyorffy, M.P. Wentland, E.V. Broude, H. Kiaris, I.B. Roninson, Cyclin-dependent kinase 8 mediates chemotherapy-induced tumor-promoting paracrine activities. *Proc Natl Acad Sci U S A* 109, 13799-13804 (2012).

20. D. B. Ring, K.W. Johnson, E.J. Henriksen, J.M. Nuss, D. Goff, T.R. Kinnick, S.T. Ma, J.W. Reeder, I. Samuels, T. Slabiak, A.S. Wagman, M.E. Hammond, S.D. Harrison, Selective glycogen synthase kinase 3 inhibitors potentiate insulin activation of glucose transport and utilization in vitro and in vivo. *Diabetes* 52, 588-595 (2003).

21. J. Bancerek, Z.C. Poss, I. Steinparzer, V. Sedlyarov, T. Pfaffenwimmer, I. Mikulic, L. Dölken, B. Strobl, M. Müller, D.J. Taatjes, P. Kovarik, CDK8 kinase phosphorylates transcription factor STAT1 to selectively regulate the interferon response. *Immunity* **38**, 250-262 (2013).

22. M.A. Burchill, J. Yang, C. Vogtenhuber, B.R. Blazar, M.A. Farrar. IL-2 receptor beta-dependent STAT5 activation is required for the development of Foxp3+ regulatory T cells. *J Immunol* **178**, 280-290 (2007).

23. L. Passerini, S.E. Allan, M. Battaglia, S. Di Nunzio, A.N. Alstad, M.K. Levings, M.G. Roncarolo, R. Bacchetta, STAT5-signaling cytokines regulate the expression of FOXP3 in CD4+CD25+ regulatory T cells and CD4+CD25- effector T cells. *Int Immunol* 20, 421-431 (2008).

24. H. Yamashita, M.T. Nevalainen, J. Xu, M.J. LeBaron, K.U. Wagner, R.A. Erwin, J.M. Harmon, L. Hennighausen, R.A. Kirken, H. Rui, Role of serine phosphorylation of Stat5a in prolactin-stimulated beta-casein gene expression. *Mol Cell Endocrinol* **183**, 151-163 (2001).

25. S. H. Park, H. Yamashita, H. Rui, D. J. Waxman, Serine phosphorylation of GH-activated signal transducer and activator of transcription 5a (STAT5a) and STAT5b: impact on STAT5 transcriptional activity. *Mol Endocrinol* **15**, 2157-2171 (2001).

26. Y. Kitagawa, N. Ohkura, Y. Kidani, A. Vandenbon, K. Hirota, R. Kawakami, K. Yasuda, D. Motooka, S. Nakamura, M. Kondo, I. Taniuchi, T. Kohwi-Shigematsu, S. Sakaguchi, Guidance of regulatory T cell development by Satb1-dependent super-enhancer establishment. *Nat Immunol* **18**, 173-183 (2017).

27 M.O. Li, A.Y. Rudensky, T cell receptor signalling in the control of regulatory T cell differentiation and function. *Nat Rev Immunol* **16**, 220-233 (2016).

28. P.A. Clarke, M.J. Ortiz-Ruiz, R. TePoele, O. Adeniji-Popoola, G. Box, W. Court, S. Czasch, S. El Bawab, C. Esdar, K. Ewan, S. Gowan, A. De Haven Brandon, P. Hewitt, S.M. Hobbs, W. Kaufmann, A. Mallinger, F. Raynaud, T. Roe, F. Rohdich, K. Schiemann, S. Simon, R. Schneider, M. Valenti, S. Weigt, J. Blagg, A. Blaukat, T.C. Dale, S.A. Eccles, S. Hecht, K. Urbahns, P. Workman, D. Wienke, Assessing the

mechanism and therapeutic potential of modulators of the human Mediator complex-associated protein kinases. *Elife* **5**, e20722 (2016).

29. J. J. Worthingto, A. Kelly, C. Smedley, D. Bauché, S. Campbell, J.C. Marie, M.A. Travis, Integrin α vβ8-Mediated TGF-β Activation by Effector Regulatory T Cells Is Essential for Suppression of T-Cell-Mediated Inflammation. *Immunity* **42**, 903-915 (2015).
30. J. P. Edwards, A. M. Thornton, E. M. Shevach, Release of active TGF-β1 from the latent TGF-β1/GARP complex on T regulatory cells is mediated by integrin β8. *J Immunol* **193**, 2843-2849 (2014).
31. A. Vandenbon, V.H. Dinh, N. Mikami, Y. Kitagawa, S. Teraguchi, N. Ohkura, S. Sakaguchi. Immuno-Navigator, a batch-corrected coexpression database, reveals cell type-specific gene networks in the immune system. *Proc Natl Acad Sci U S A* **113**, E2393-2402 (2016).
32. G. Cheng, X. Yuan, M.S. Tsai, E.R. Podack, A. Yu, T.R. Malek, IL-2 receptor signaling is essential for the development of Klrg1+ terminally differentiated T regulatory cells. *J Immunol* **189**, 1780-1791 (2012).
33. X. Li, Y. Liang, M. LeBlanc, C. Benner, Y. Zheng, Function of a Foxp3 cis-element in protecting regulatory T cell identity. *Cell* **158**, 734-748 (2014).
34. G. Lal, J.S. Bromberg, Epigenetic mechanisms of regulation of Foxp3 expression. *Blood* **114**, 3727-3735 (2009).
35. J. Nemet, B. Jelicic, I. Rubelj, M. Sopta, The two faces of Cdk8, a positive/negative regulator of transcription. *Biochimie* **97**, 22-27 (2014).
36. T. Rzymski, M. Mikula, E. Żyłkiewicz, A. Dreas, K. Wiklik, A. Gołas, K. Wójcik, M. Masiejczyk, A. Wróbel, I. Dolata, A. Kitlińska, M. Statkiewicz, U. Kuklinska, K. Goryca, Ł. Sapała, A. Grochowska, A. Cabaj, M. Szajewska-Skuta, E. Gabor-Worwa, K. Kucwaj, A. Białas, A. Radzimierski, M. Combik, J. Woyciechowski, M. Mikulski, R. Windak, J. Ostrowski, K. Brzózka, SEL120-34A is a novel CDK8 inhibitor active in AML cells with high levels of serine phosphorylation of STAT1 and STAT5 transactivation domains. *Oncotarget* **8**, 33779-33795 (2017).
37. M.D. Galbraith, A.J. Donner, J.M. Espinosa, CDK8: a positive regulator of transcription. *Transcription* **1**, 4-12 (2010).
38. M. Chen, J. Liang, H. Ji, Z. Yang, S. Altilia, B. Hu, A. Schronce, M.S.J. McDermott, G.P. Schools, C.U. Lim, D. Oliver, M.S. Shtutman, T. Lu, G.R. Stark, D.C. Porter,

E.V. Broude, I.B. Roninson, CDK8/19 Mediator kinases potentiate induction of transcription by NFκB. *Proc Natl Acad Sci U S A* **114**,10208-10213 (2017).

39. J. Liang, M. Chen, D. Hughes, A.A. Chumanevich, S. Altilia, V. Kaza, C.U. Lim, H. Kiaris, K. Mythreye, M.M. Pena, E.V. Broude, I.B. Roninson, CDK8 Selectively Promotes the Growth of Colon Cancer Metastases in the Liver by Regulating Gene Expression of TIMP3 and Matrix Metalloproteinases. *Cancer Res* **78**, 6594-6606 (2018).
40. M Miyara, Y. Yoshioka, A. Kitoh, T. Shima, K. Wing, A. Niwa, C. Parizot, C. Taflin, T. Heike, D. Valeyre, A. Mathian, T. Nakahata, T. Yamaguchi, T. Nomura, M. Ono, Z. Amoura, G. Functional delineation and differentiation dynamics of human CD4+ T cells expressing the FoxP3 transcription factor. *Immunity* **30**, 899-911 (2009).

Acknowledgments: We thank M. Hattori (Kyoto University Graduate School of Medicine), K. Tamura, N. Morikawa, R. Murakami, A. Katoh (Astellas Pharma Inc.) for constructive discussion, E. Moriyoshi, T. Ushitani, and S. Chuganji for their technical assistance, and A. Tanaka (Hyogo University of Health Science) for providing the Linker compound.

Funding: This work was supported by the Special Coordination Funds by the Ministry of Education, Culture, Sports, Science and Technology of Japan and Astellas Pharma Inc.

Author contributions: M.A., N.M., N.O., Y.M., I.A., S.N. and S.S. designed the study; N.N. and S.U. performed the chemical-biology experiments; M.A., N.M., N.O., R.K., Y.K., A.S., K.H. and G.X. performed the cell-biology experiments; T.K., H.H. and H.H. performed the medicinal-chemistry experiments; M.A., M.N., R.K., N.N., S.U., G.X., T.K., H.H. and H.H. planned the experiments and analyzed the data. All the authors discussed the results and edited the manuscript written by M.A., M.N., S.N., and S.S.

Competing interests: M.A, N.N, S.U, T.K, H.H, H.H, Y.M and I.A. are employees of Astellas Pharma Inc. S.N. is a scientific advisor to Astellas Pharma Inc. S.S., N.O., N.M., S.N., M.A., G.X., H.H., N.N., S.U. and H.H. are the authors on a patent application related to this work placed by Kyoto University and Astellas Pharma Inc., (PCT/JP2018/2826). No potential conflicts of interest were disclosed by the other authors.

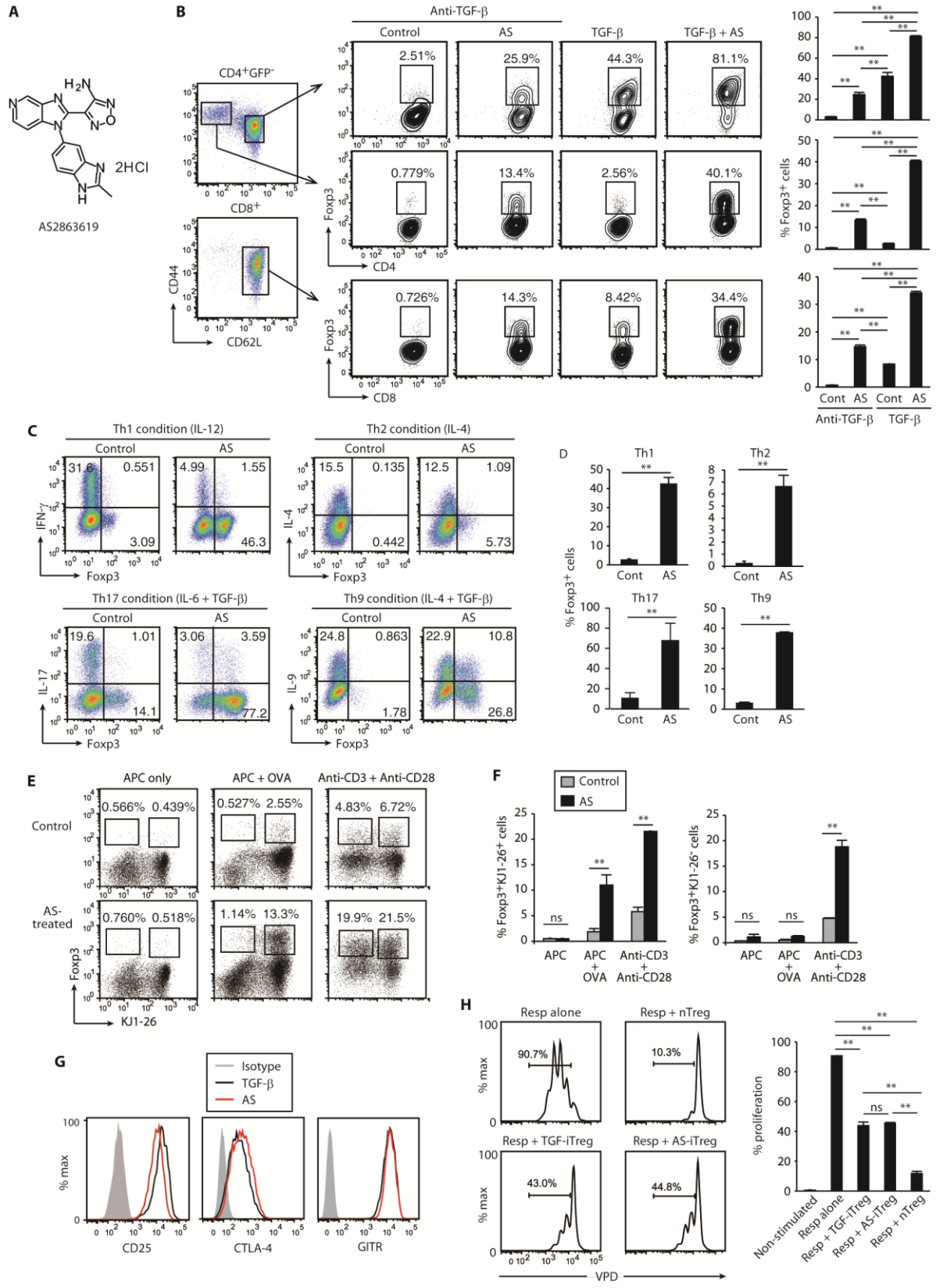

Fig. 1. AS2863619 as a potent Foxp3 inducer in Tconv cells. (**A**) Chemical structure of AS2863619, hereafter designated AS. **(B)** In vitro induction of Foxp3 expression in AS-treated mouse effector/memory and naïve $CD4^+$ T cells as $CD44^{high}CD62L^{low}$ and

$CD44^{low}CD62L^{high}$ cells, respectively, and also in $CD8^+$ T cells. Cells were stimulated with anti-CD3/CD28 mAb-coated beads and IL-2 in the presence or absence of AS (1.0 μM) or TGF-β (2.5 ng/ml) for 72 hours. Representative Foxp3 staining and percentages of $Foxp3^+$ cells among $CD4^+$ or $CD8^+$ T cells after respective stimulation are shown (n=3). **(C** and **D)** $Foxp3^+$ cells generation by AS under a Th1-, Th2-, or Th17-inducing condition. Naïve $CD4^+$ T cells were anti-CD3/CD28-stimulated in the presence of 10 ng/ml IL-12 (Th1 condition, n=5), 10 ng/ml IL-4 (Th2 condition, n=4), 20 ng/ml IL-6+2.5 ng/ml TGF-β (Th17 condition, n=4), or 10 ng/ml IL-4+2.5 ng/ml TGF-β (Th9 condition, n=3). **(E** and **F)** $Foxp3^+$ T-cell generation from antigen-stimulated T cells. DO11.10 naïve $CD4^+$ T cells were co-cultured with APCs, 5 μM OVA peptide, and 1.0 μM AS, and assessed for Foxp3 and DO11.10 TCR expression by flow cytometry (n=3). **(G)** Expression of Treg signature molecules in AS- or TGF-β-treated anti-CD3/CD28-stimulated T cells assessed by flow cytometry. Representative of three independent experiments. **(H)** *In vitro* suppression assay by using *in vitro* activated nTreg cells and TGF-β- or AS-induced iTreg cells (n=3). Treg versus responder T cell ratio was 1:10. Vertical bars indicate means ± SD. $^{**}P < 0.01$, $^{*}P < 0.05$ (SNK method).

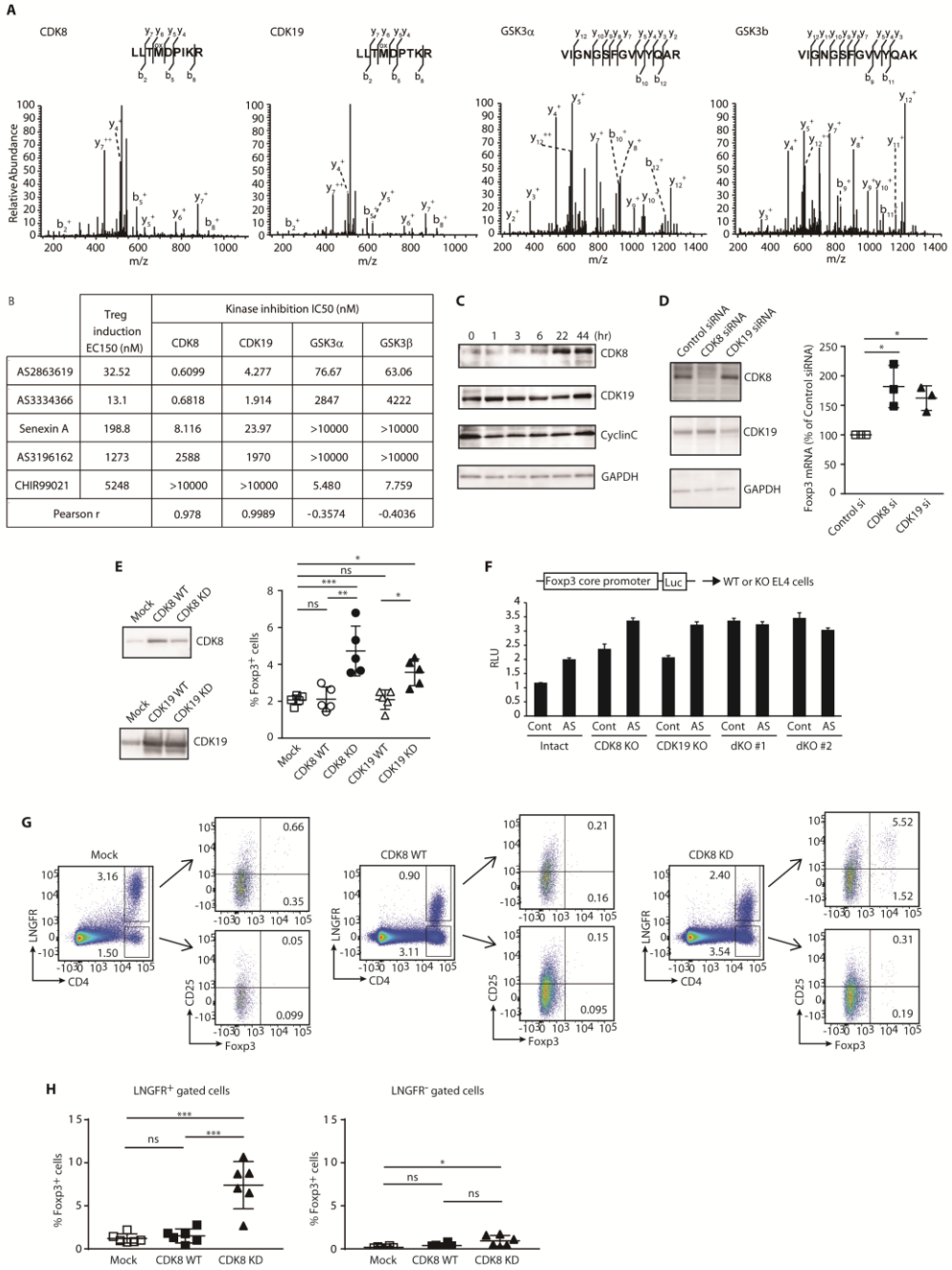

	Treg induction EC150 (nM)	Kinase inhibition IC50 (nM)			
		CDK8	CDK19	GSK3α	GSK3β
AS2863619	32.52	0.6099	4.277	76.67	63.06
AS3334366	13.1	0.6818	1.914	2847	4222
Senexin A	198.8	8.116	23.97	>10000	>10000
AS3196162	1273	2588	1970	>10000	>10000
CHIR99021	5248	>10000	>10000	5.480	7.759
Pearson r		0.978	0.9989	-0.3574	-0.4036

Fig. 2. CDK8/19 as a key target of AS. (**A**) Candidate target molecules of AS revealed by tandem mass spectrometry (**fig. S6**). (**B**) Correlation of Treg induction with the degree of CDK8/19 kinase inhibition. Five different kinase inhibitors including AS were examined for their Treg-inducing potency and their inhibitory activity of various kinases. Kinase inhibition was assessed *in vitro* using recombinant CDK8/cyclin C complex, CDK19/cyclin C complex, GSK3α or GSK3β. IC50 was defined as the concentration of an inhibitor that reduced phosphorylation by half compared to DMSO control. EC150 for Treg induction was defined as the concentration of compound that induced Foxp3$^+$ Treg cells to 150% of DMSO control when mouse naive CD4$^+$ T cells were treated with anti-CD3/CD28 for 44 hours in the

presence of the compound. Values are geometric mean of three (Treg induction, CDK19, GSK3α, GSK3β) or four (CDK8) independent experiments. Pearson r, Pearson's correlation coefficient (vs Treg induction). (**C**) Expression of CDK8, CDK19 and Cyclin C after stimulation. Mouse $CD4^+$ T cells stimulated with anti-CD3/CD28 were lysed for immuno-blotting of these molecules at various time points. Representative of three independent experiments. (**D**) The effects of CDK8 or CDK19 knock-down on Foxp3 mRNA expression. Mouse $CD4^+$ T cells were transfected with siRNA for CDK8 or CDK19, stimulated with anti-CD3/CD28, TGF-β, and IL-2 and examined for CDK8 and CDK19 expression by immuno-blotting (left), or Foxp3 mRNA expression by quantitative RT-PCR (n=3) (right). (**E**) The effects of retroviral expression of WT or kinase-dead (KD) CDK8 or CDK19 on $Foxp3^+$ cell generation. Mouse $CD4^+$ T cells infected with retrovirus harboring GFP (mock control), WT or KD CDK8, WT or KD CDK19 gene, were stimulated with anti-CD3/CD28 and IL-2, and examined for CDK8 and CDK19 expression by immuno-blotting (left panel) and for the percentages of $Foxp3^+$ cells among $CD4^+$ T cells by flow cytometry (n=5) (right panel). **(F)** Luciferase assay using CDK8 and/or CDK19 KO EL4 cell lines and a Foxp3 promoter plasmid (triplicate). Representative of two independent experiments. (**G** and **H**) Foxp3 induction in CDK8-KD-transfected $CD4^+$ T cells by antigenic stimulation. Naive $CD4^+$ T cells isolated from DO11.10$Rag2^{-/-}$Foxp3-eGFP reporter mice were stimulated with anti-CD3/CD28 for 22 hours, infected with mock or CDK8-KD or -WT-carrying retroviruses, incubated for another 22 hours in the absence of IL-2, and rested for 10 days in the presence of 100 U/mL IL-2. LNGFR was used as a marker of infection. BALB/c-nu/nu mice were transferred with infected T cells on day 0, and treated with IL-2/anti-IL-2 Ab complexes on day 7, and then immunized with OVA/CFA on day 14. Draining lymph nodes were collected and examined for expression of Foxp3 by flow cytometry on day 20. Representative staining (**G**) and percentages of $Foxp3^+$ cells among live $LNGFR^+$ or $LNGFR^-CD4^+$ cells in lymph nodes are shown (n=6) (**H**). Vertical bars indicate means ± SD. ***P < 0.001, **P < 0.01, *P < 0.05 (Dunnett's test). ns, not significant.

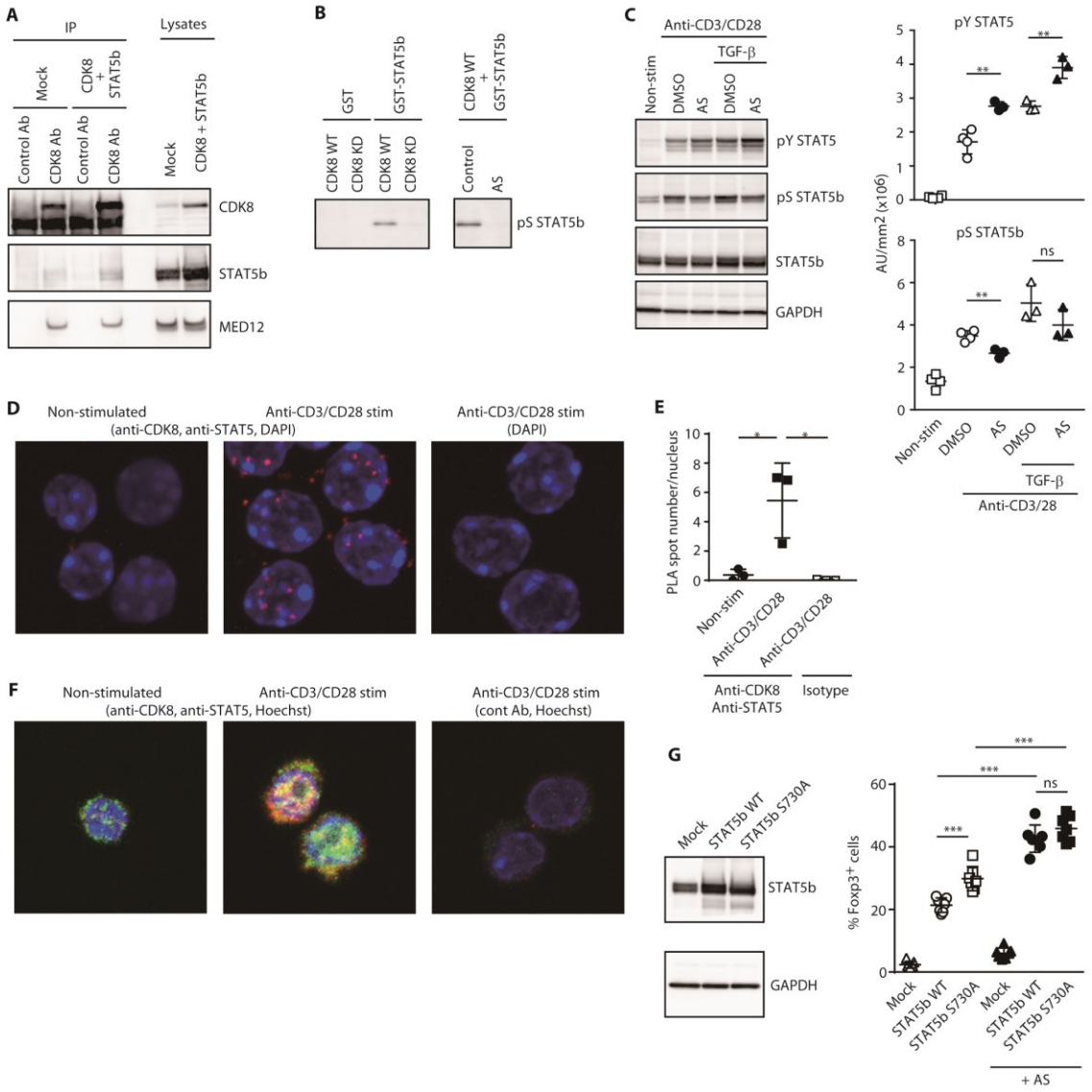

Fig. 3. Interaction of CDK8/19 and STAT5 in inducing Foxp3 expression. (**A**) Mouse $CD4^+$ T cells were mock-infected or infected with retrovirus harboring the WT CDK8 and STAT5b genes, stimulated with anti-CD3/CD28 and IL-2, and subjected to immuno-precipitation and immunoblotting for CDK8, STAT5b and MED12. Representative of two independent experiments. (**B**) STAT5 serine phosphorylation by CDK8. Recombinant GST-STAT5b incubated with recombinant WT or KD CDK8 in the presence or absence of 1.0 μM AS, with 100 μM ATP and 10 mM $MgCl_2$ was subjected to immunoblotting for phospho-serine (pS) of STAT5b. Representative of two independent experiments. (**C**) Control of serine and tyrosine phosphorylation by AS in activated T cells. Mouse $CD4^+$ T cells were stimulated with anti-CD3/CD28 in the presence or absence of TGF-β for 22 hours, in the absence (DMSO) or presence of 100 nM AS, lysed and subjected to immunoblot analysis for

STAT5b, pS-STAT5b or pY-STAT5. Signal intensity was quantified and normalized by GAPDH (n=3 or 4). **P<0.01 (t-test). ns, not significant. (**D** and **E**) Mouse naive $CD4^+$ T cells were incubated in the presence or absence of anti-CD3/28 for 22 hours, and proximity ligation assay was performed to assess interaction between CDK8 and STAT5. Images were obtained using LSM710 confocal microscope. Data were presented as maximum intensity projection (n=3). Each red spot represents for a single interaction and DNA was stained with DAPI. (**F**) Mouse naive $CD4^+$ T cells were incubated in the presence or absence of anti-CD3/CD28 for 22 hours, and examined for expression of CDK8 and STAT5. DNA was stained with Hoechst33342. Images were obtained using LSM710 confocal microscope. Representative of two independent experiments. (**G**) Mouse $CD4^+$ T cells infected with retrovirus encoding WT or S730A mutant STAT5b were stimulated with anti-CD3/CD28 and IL-2, without TGF-β, and subjected to immunoblotting for STAT5b (left panel), or assessed for the percentage of $Foxp3^+$ cells among live virus-infected (i.e., GFP^+) $CD4^+$ T cells by flow cytometry (n=7) (right panel). ***P<0.001 (t-test). ns, not significant.

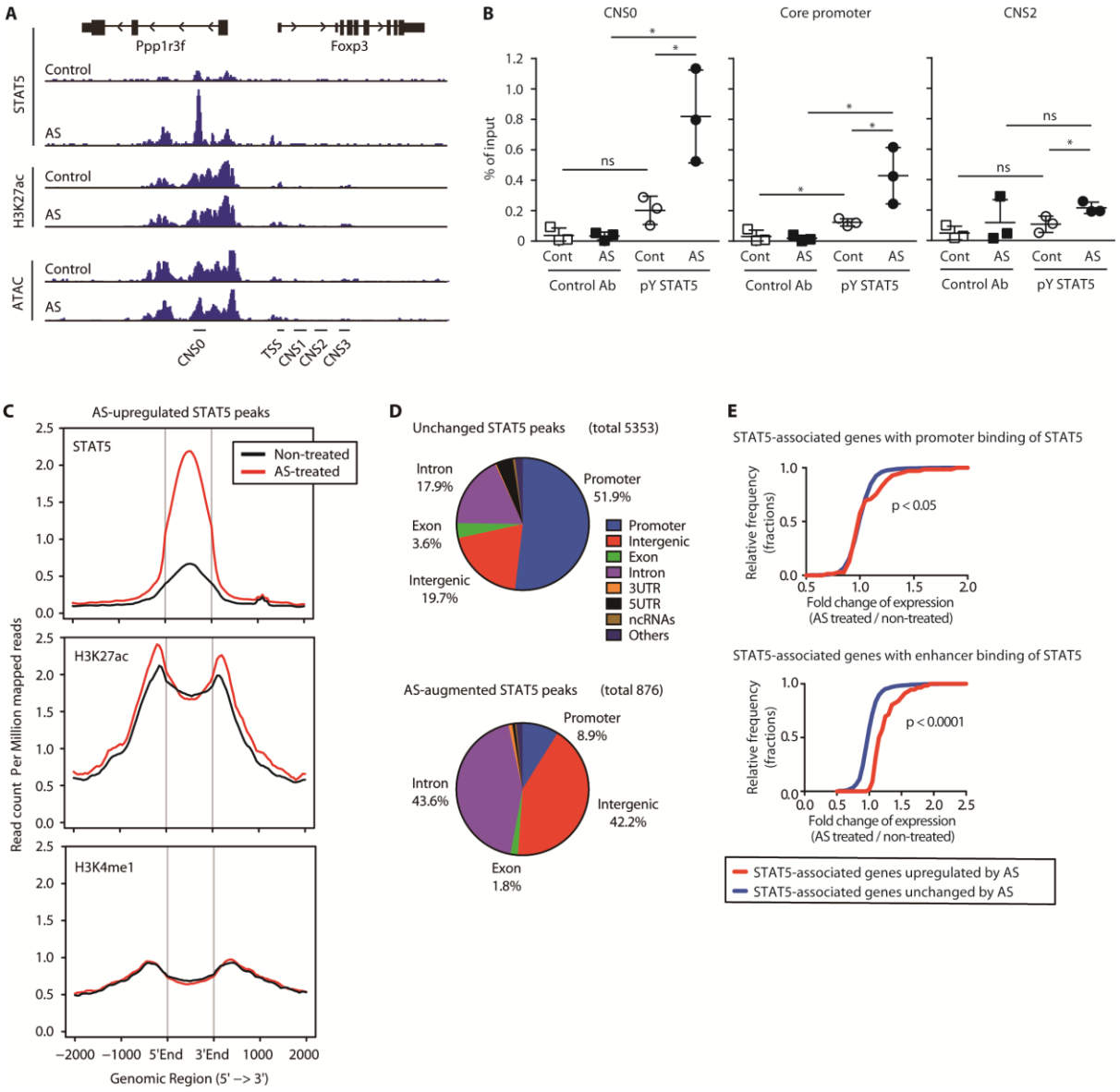

Fig. 4. Genome-wide enhancement of STAT5-dependent gene expression by AS. (A) Mouse CD4$^+$ T cells stimulated with anti-CD3/CD28 with or without 1.0 μM AS were analyzed at the Foxp3 gene locus for STAT5 binding, H3K27ac, and chromatin status by ChIP-seq and ATAC-seq. (**B**) Mouse CD4$^+$ T cells stimulated with anti-CD3/CD28 and TGF-β with or without 1.0 μM AS were subjected to ChIP-qPCR assay for pY-STAT5 binding at Foxp3 CNS0, CNS2, and core promoter regions (n=3). *P<0.05, ns, not significant. (**C**) Density of STAT5 binding and indicated histone modifications in AS-treated or non-treated T cells. Normalized ChIP-seq signal density is plotted for AS-upregulated STAT5-binding sites ± 2 kb. (**D**) STAT5 binding peaks were separated into two groups, i.e., unchanged or up-regulated peaks after AS treatment, and the frequency of the peaks locating in promoter, intron, exon, intergenic, 3'UTR or 5'UTR of mRNAs, non-cording RNAs (ncRNA), and

others was calculated in each group by using annotatePeaks.pl of homer v4.8 in default settings. (**E**) Cumulative histogram of fold change on average (AS-upregulated vs AS-unchanged STAT5 peak sites) of three independent RNA-seq results. STAT5 binding Peaks were classified into proximal promoter or enhancer regions (within 1000 base in H3K4me1 or H3K27ac positive region). Statistical significance was determined by the Kolmogorov-Smirnov test.

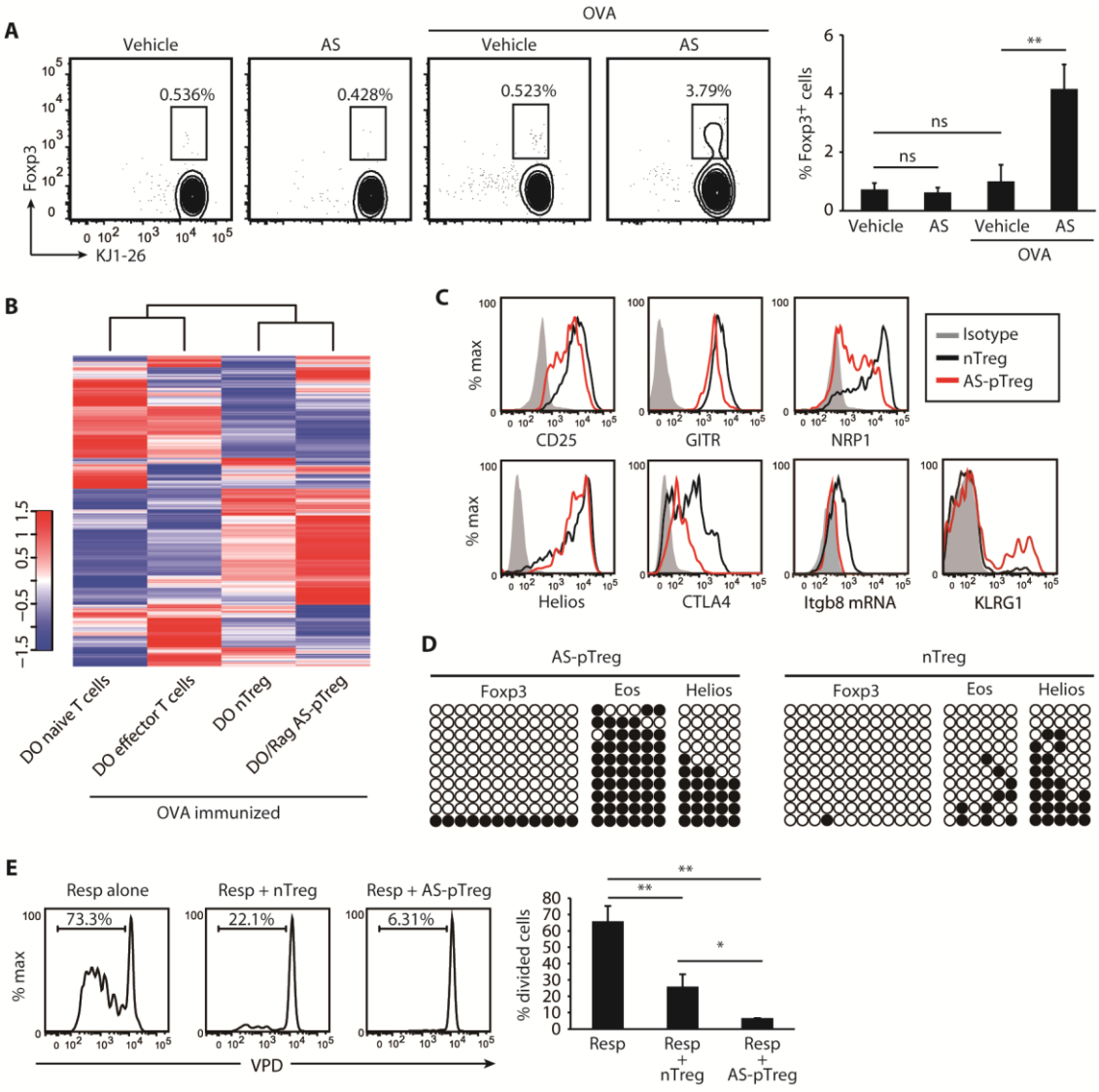

Fig. 5. *In vivo* induction of antigen-specific pTreg cells by AS. (A) Flow cytometry of Foxp3$^+$ cells in DO11.10RAG2$^{-/-}$Foxp3-eGFP reporter mice with or without subcutaneous OVA immunization. CD4$^+$ T cells in the draining lymph nodes of mice treated orally with 30 mg/kg AS every day for 7 days were stained for Foxp3 on day 8. Representative staining (left panel) and percentages of Foxp3$^+$ cells among CD4$^+$ T cells (n=6) (right panel). (**B**) The gene expression pattern of Foxp3$^+$ T cells from OVA- and AS- treated DO11.10RAG2$^{-/-}$Foxp3-eGFP reporter mice (designated as DO/Rag AS-pTreg), as shown in (**A**), compared with Foxp3$^+$ T cells (DO nTreg) and Tconv cells (DO effector T cells) in OVA-immunized DO11.10 mice, or Tconv cells (DO naiveT cells) in OVA-nonimmunized mice. Heat map shows the expression of Treg signature genes analyzed by RNA-seq. Hierarchical cluster analysis was conducted on all expressed genes. (**C**) Flow cytometry of Treg signature molecules expressed by AS-induced Treg cells (AS-pTreg) in (**A**) or nTreg cells from OVA-

immunized DO.11.10 mice. Itgb8 expression was assessed by mRNA staining. Representative of at least three experiments. (**D**) Bisulfite sequencing showing Treg-specific demethylated regions at Foxp3 CNS2, Eos int1b and Helios int3a. Representative of 2~4 experiments. (**E**) Suppression assay performed by co-culturing of VPD-labeled responder $CD4^+$ T cells, APCs and nTreg or pTreg cells, shown in (**A**), in the presence of soluble anti-CD3 mAb. Representative result (left panel) and total results (n=3) (right panel). Vertical bars indicate means ± SD. Statistical significance was assessed by the SNK method, Student's t test, or Kaplan-Meier method. $^{**}P < 0.01$, $^{*}P < 0.05$.

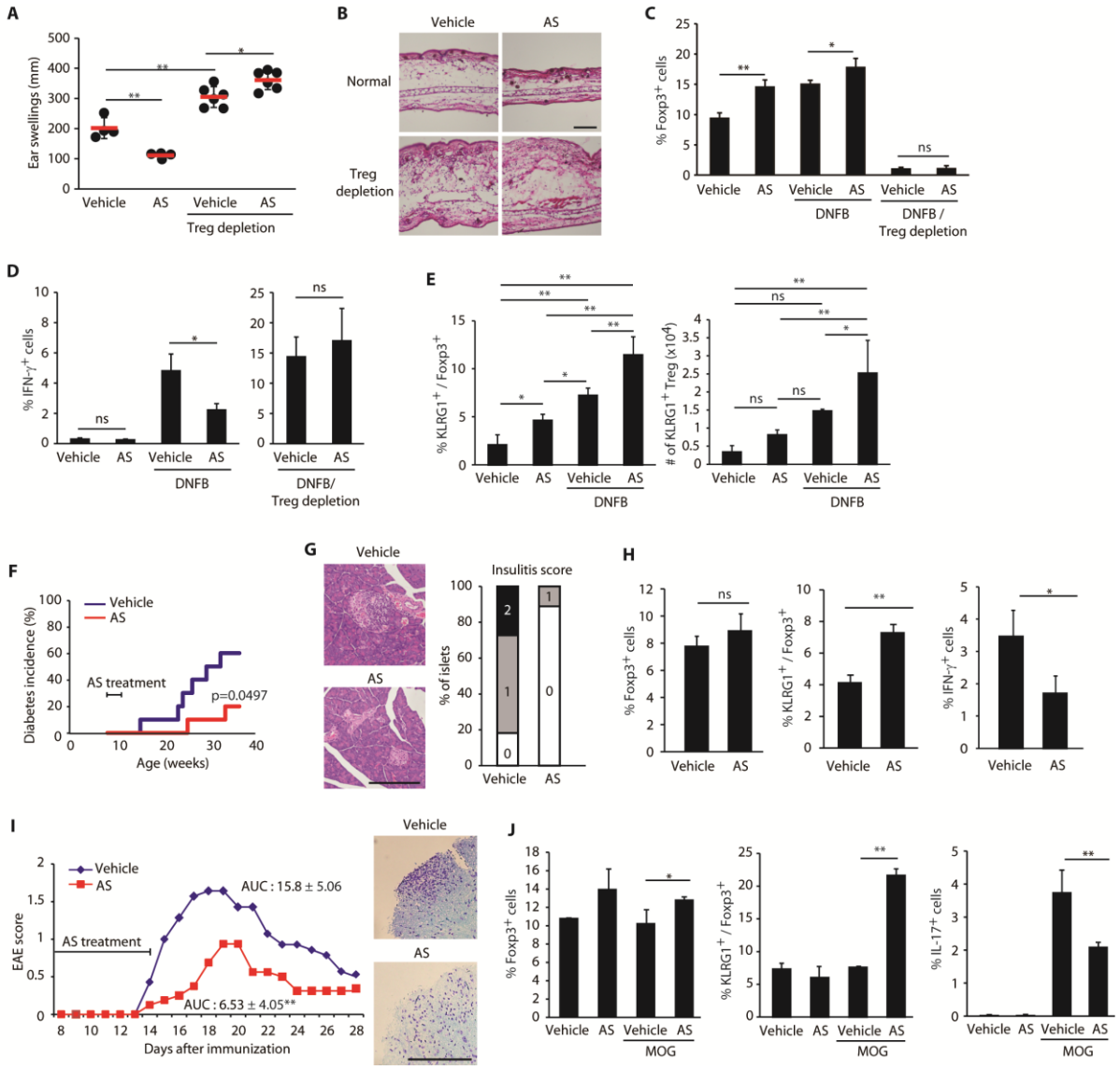

Fig. 6. Therapeutic effects of AS on autoimmunity and allergy. (A-E) AS treatment of DNFB-induced contact skin hypersensitivity. Mice expressing diphtheria-toxin receptor under the Foxp3 promoter were sensitized epicutaneously with DNFB on the abdominal skin on day 0 and 7, challenged on day 14 by applying DNFB on the ear, while some of them were orally administered with AS (30 mg/kg) daily for 2 weeks (n=4). A group of the mice (n=6) were also treated with diphtheria toxin daily from days 0 to 14 to deplete $Foxp3^+$ cells. Ear swelling was measured 24 hours after challenge (**A**), with preparation of histology (H&E staining) (**B**). Percentages of $Foxp3^+$ cells (**C**) and IFN-γ^+ cells (**D**) among $CD4^+$ T cells and $KLRG1^+$ cells among $Foxp3^+CD4^+$ T cells (**E**) in the regional lymph nodes on day 14 (n=3 or 4). (**F**) AS treatment of NOD mice. NOD mice (n=10) were daily treated orally with AS (30 mg/kg) from 8 to 10 weeks of age, and assessed for urinary glucose once a week (left panel). Histological severity of insulitis was scored from 0 to 2 at 10 weeks of age (n=9-11) (middle and right panels). (**G**) Percentages of $Foxp3^+$ T cells among $CD4^+$ T cells and

KLRG1^{+}Foxp3^{+}CD4^{+} T cells among Foxp3^{+}CD4^{+} T cells in the regional lymph nodes of NOD mice (n=4) were assessed by flow cytometry. (**H**) Percentage of IFN-γ^{+} T cells in the regional lymph nodes of 10-week-old NOD mice (n=4) were assessed by flow cytometry. (**I** and **J**) EAE was induced by MOG immunization and AS (30 mg/kg) was daily administered from day 0 to day 14 (n=7 or 8 per group). (**I**) EAE clinical scores and histology of spinal cords were assessed from day 8 to 28 after immunization. Spinal cords from EAE-induced mice were stained with Luxol fast blue. Percentage of Foxp3^{+}, KLRG1^{+} and IL-17^{+} cells (**J**) among CD4+ T cells in the regional lymph nodes were analyzed by flow cytometry on day 14 (n=3 or 4). Vertical bars indicate means ± SD. Statistical significance was assessed by the SNK method, Student's t test, or Kaplan-Meier method. $^{**}P < 0.01$, $^{*}P < 0.05$.

Supplementary Materials for

Conversion of antigen-specific conventional T cells into Foxp3-expressing Treg cells by inhibition of Cdk8/19

Masahiko Akamatsu[1,4†], Norihisa Mikami[2,3†], Naganari Ohkura[2], Ryoji Kawakami[2], Yohko Kitagawa[2], Atsushi Sugimoto[2], Keiji Hirota[3], Naoto Nakamura[4], Satoru Ujihara[4], Toshio Kurosaki[4], Hisao Hamaguchi[4], Hironori Harada[4], Guliang Xia[5], Yoshiaki Morita[1,4], Ichiro Aramori[1,4], Shuh Narumiya[1]*, Shimon Sakaguchi[2,3]*

correspondence to: snaru@mfour.med.kyoto-u.ac.jp, shimon@ifrec.osaka-u.ac.jp

This PDF file includes:

Materials and Methods

Figures S1-S19

Tables S1-S2

Supplementary Materials:

Materials and Methods

Mice

C57BL/6, BALB/c, NOD and BALB/c-nu/nu mice were purchased from SLC or CLEA. DO.10.11 TCR transgenic mice, RAG2 deficient mice, Foxp3-DTR-GFP (FDG) and Foxp3-eGFP (eFox) reporter mice have been already described (*41-43*). All procedures were in accordance with the National Institutes of Health Guide for the Care and Use of Laboratory Animals and approved by the Committee on Animal Research of Kyoto University Faculty of Medicine or Osaka University.

Antibodies and reagents

Antibodies were listed on **Table S2**. AS2863619, AS3334366, AS3196162, AS3293990 and AS3309191 were synthesized by Astellas Pharma Inc (Chemical structures of these compounds were shown in **Fig. 1A** and **fig. S6**). CHIR99021 and CP690550 were purchased from Selleckchem; Senexin A, NFAT inhibitor (CAS:249537-73-3) and SP 100030 (AP-1/NF-κB Dual Inhibitor) from Tocris Bioscience; rapamycin from Cell Signaling Technology; STAT5 inhibitor (CAS:285986-31-4), GSK-3β Inhibitor (CAS:99-73-0), Foxo1 Inhibitor (CAS:836620-48-5) and BAY-11-7082 from Cayman Chemical Company; all trans-retinoic acid and dexamethasone from Sigma; OVA (323-339) and MOG (35-55) peptides from MBL. For the enrichment of $CD4^+$ cells, $CD4^+$ T cell Isolation kit, human (MIltenyi Biotec), and Mouse CD4 T Lymphocyte Enrichment Set (BD) were used. For intracellular cytokine staining, Cell Stimulation Cocktail (plus protein transport inhibitors) (eBioscience) was used. StemXVivo Serum-Free Human T Cell Base Media (R&D Systems) was used for serum-free culture.

Cell sorting and in vitro cell culture

T cell sorting and culture were performed as previously described (*44*). Briefly, lymph node cells derived from eFox mice were stained with antibodies. Then $CD4^+GFP^+$ cells were sorted as nTreg cells and $CD4^+GFP^-CD44^{low}CD62L^{high}$ cells were sorted as naïve T cells by FACSAriaII (BD). In some experiments, $CD4^+GFP^-CD44^{high}CD62L^{low}$ cells were prepared as effector/memory T cells.

For cell culture, we used RPMI1640 supplemented with 10% FCS (v/v), 60 μg/mL penicillin G, 100 μg/mL streptomycin, 0.1 mM 2-mercaptoethanol. Sorted T cells were

stimulated by using Dynabeads Mouse T-Activator CD3/CD28 in the presence of 50 U/ml of IL-2.

In co-culture assay, 2×10^5 $CD4^+$ DO11.10 T cells were plated with 4×10^4 T-cell-depleted splenocytes in the presence of 5 μM of OVA peptide. AS was used at 1.0 μM, except where noted.

CFSE or violet proliferation dye (VPD) labeling was performed by incubating with 5 μM reagents at room temperature for 5 min. Labeling reaction was quenched by adding 5 volumes of cold medium and incubated for 20 min on ice. After washing, cells were stimulated and proliferation was determined by FACS.

Human $CD4^+$ T cells were purified from PBMCs of healthy donors. Pre-enriched PBMCs were stained with anti-CD4, anti-CD25 and anti-CD45RA mAb for 30 min on ice. After washing, $CD4^+CD25^-CD45RA^+$ cells were sorted by FACSAriaII. Cells were cultured with IL-2 (50 U/ml) and Dynabeads Human T-Activator CD3/CD28 in the presence or absence of AS. All donors provided written informed consent before sampling according to the Declaration of Helsinki. The present study was approved by the institutional ethics committees of Osaka University.

Flow cytometry analysis

Flow cytometry analysis was performed as previously described (*44*). Cytokine staining was carried out following incubation of cells with Cell Stimulation Cocktail (eBioscience) for 4 hours at 37°C. Cells were fixed by eBioscence Foxp3 / Transcription Factor Staining Buffer Set or BD Pharmingen Transcription Factor Buffer Set according to the manufacturer's instructions.

Flow cytometric *in situ* hybridization of integrin β8 mRNA was carried out by PrimeFlow RNA Assay (eBioscience) according to the manufacturer's instructions.

CpG methylation analysis by bisulfite sequencing

Bisulfite sequencing analysis was performed as previously described (*14*). Cells were collected by FACSAriaII and DNA was extracted by phenol extraction and ethanol precipitation. Bisulfite reaction was carried out using the MethylEasy Xceed Rapid DNA Bisulphite Modification Kit (Human Genetic Signatures).

Affinity purification using chemical probes and protein identification

EL4 cells were purchased from DS pharma biomedical and maintained in DMEM (Thermo Fisher Scientific) supplemented with 10% FCS (SIGMA). Pull down experiment and mass spectrometry analyses were performed as previously described (*15*). Cell lysate was made from EL4 lysed in 0.2% CHAPS lysis buffer (0.2% CHAPS, EDTA-free Protease Inhibitor in HBS-N). Tool compound was coupled to the photoreactive affinity capture linker by amine coupling using *O*-(1*H*-benzotriazole-1-yl)-1,1,3,3-tetramethyluronium tetrafluoroborate and 1-hydroxybenztriazole.

Treg cell induction EC150

Mouse naive $CD4^+$ T cells were purified with mouse naive $CD4^+$ T Cell Isolation Kit (Miltenyi) from spleens of C57BL6. T cells were cultured in RPMI 1640 (Thermo Fisher Scientific) supplemented with 10% FCS (SIGMA), 2-mercapthoethanol (SIGMA) and 50 μg/ml streptomycin and 50 U/ml penicillin (Thermo Fisher Scientific). To induce mouse iTreg cells, mouse naive $CD4^+$ T cells were cultured with Dynabeads Mouse T-Activator CD3/CD28 (Thermo Fisher Scientific) at a bead-to-cell ratio of 1:1 for 44 hours. The cells were then stained with anti-mouse CD4 and anti-mouse Foxp3 mAbs and were analyzed by flow cytometry. EC150 was defined as the concentration of compounds that induced 150 % of $Foxp3^+$ $CD4^+$ cells compared to DMSO control. When EC150 couldn't be calculated, the maximum concentration of compounds evaluated in this assay (10 μM) was used for the calculation of the geometric mean.

RNA interference (RNAi) in mouse $CD4^+$ T cells

RNAi in mouse $CD4^+$ T cells was achieved by transfection with GenomONE-Si (Ishihara Sangyo) and a pre-designed small interfering RNAs (siRNAs) were purchased from Thermo Fisher Scientific (Negative control siRNA, CDK8 siRNA, ID# s113914; CDK19 siRNA, ID#s95476,) according to the manufacturer's instructions. Mouse $CD4^+$ T cells were purified with CD4 (L3T4) MicroBeads (Miltenyi) from spleens of C57BL6. The cells were transfected with 250 nM siRNA, and stimulated by plate-bound anti-CD3/CD28. After 24 hours, the cells were transfected again with siRNAs, and incubated for another 24 hours. After samples were collected for immunoblotting, the cells were stimulated with 5 ng/mL TGF-β and 250 U/mL IL-2 (R and D systems) and Dynabeads Mouse T-Activator CD3/CD28 for 22 hours. RNA was isolated from T cells by using RNeasy plus micro kit

(Qiagen), and cDNA was prepared with SuperScript VILO cDNA Synthesis Kit (Thermo Fisher Scientific). RT-PCR was performed by using Taqman Fast Advanced Master Mix (Thermo Fisher Scientific) and pre-designed Taqman probe sets were purchased from Thermo Fisher Scientific (18S, Mm03928990_g1, Foxp3, Mm00475162_m1). Foxp3 expression level was normalized by 18S rRNA.

Retroviral transduction

A fragment encoding mouse CDK8, CDK19 or STAT5b cDNA was obtained from pCMV6-CDK8 (Origene, MR218219), pCMV6-CDK19 (Origene, MR215712) or pCMV6-STAT5b (Origene, MR210649) and subcloned into a retroviral plasmid pMCs-IRES-GFP (Cell Biolabs). D173A mutation of CDK8 or CDK19 (45, 46) were induced with primers as follows: CDK8 D173A Forward: GAGTAAAAATTGCTGCCATGGGCTTTGCCCG, CDK8 D173A Reverse: CGGGCAAAGCCCATGGCAGCAATTTTTACTC, CDK19 D173A Forward: GAGTCAAAATAGCTGCCATGGGTTTTGCCAG, CDK19 D173A Reverse: CTGGCAAAACCCATGGCAGCTATTTTGACTC. S730A mutation of STAT5b was induced with primers as follows: STAT5b S730A Forward: ATGGATCAGGCTCCTGCCCCAGTCGTGTGCC, STAT5b S730A Reverse: GGCACACGACTGGGGCAGGAGCCTGATCCAT. Gene transduction of retroviral constructs into mouse $CD4^+$ T cells was performed by stimulating cells by plate-bound anti-CD3/CD28. After 24 hours culture, activated T cells were infected with viral supernatants supplemented with 5 mg/ml polybrene, followed by centrifugation for 1 hour at 3200 rpm. Infected cells were then stimulated with Dynabeads Mouse T-Activator CD3/CD28 and IL-2 (250 U/mL) for 44 hours. The cells were stained with PE-Cy7-labeled anti-Mouse CD4, APC-Cy7-labeled anti Mouse-CD25 and APC-labeled anti-Mouse Foxp3 and were analyzed by flow cytometry. The rest of the cells were lysed for immunoblotting for CDK8 and CDK19. For the assessment of interaction between CDK8 and STAT5b, cell lysates were subjected to immuno-precipitation with anti-CDK8 or rabbit isotype control Ab with Dynabeads Protein A (Thermo Fisher Scientific).

Luciferase reporter assay

Luciferase reporter assay was carried out by using Picagene Dual Seapangy Luminescence kit (Promega). Briefly, 1.6 μg PGL4.10-luciferase vectors were transfected into 1×10^6 EL4 cells by using Nucleofector Amaxa Cell Line Nucleofector Kit L (Lonza) according to the manufacturer's instructions. After 24 hours, cells were stimulated with Dynabeads Mouse T-Activator CD3/CD28 and AS (1 μM) for another 24 hours. Luc activity was recorded using the GLOMAX Luminometer (Promega).

Establishment of Cdk8/19 KO EL4 cells

Designed guide RNAs were ligated into pSpCas9-T2A-GFP/sgRNA (original vector was kindly supplied by Feng Zhang (pSpCas9n(BB)-2A-GFP (PX461), Addgene plasmid # 48140), ref. (*47*)) after BbsI digestion. Guide RNA sequences are described below.

sgCDK8; AAGTTGGTCGAGGCACTTAC

sgCDK19; GAGGATCTGTTTGAGTACGA

Cas9 and sgRNA expression vectors were transfected into EL4 cells, using the Nucleofector L system (Lonza). After sorting of GFP^+ cells by FACSAriaII, cells were diluted into single cell suspension and clonally expanded by maintaining in culture medium with Penicillin/Streptomycin for 1-2 weeks. Target deletion was confirmed by western blot and DNA sequencing.

Immunoblotting

Antibody binding on PVDF membrane (Immobilon P, Merck Millipore) was detected by using the ECL prime Western Blotting Detection Reagent (GE healthcare) and Image Quant LAS4000 system (FujiFilm). Signal intensity was quantified and normalized with GAPDH by using MaltiGauge 3.2 (Fiji Image Analyzing).

RNA-sequencing analysis

For in vitro Foxp3 induction, 1×10^6 naïve T cells were cultured in the 1 mL of 10% FCS-supplemented RPMI1640 medium, with the stimulation of 25 μL of Dynabeads Mouse T-Activator CD3/CD28 and 50 U/mL (final concentration) of IL-2 for 18 hours followed by AS treatment for 6 hours. $CD19^+$ B cells and BMDCs were cultured in the same condition for 18 hours followed by AS treatment for 6 hours. For in vivo pTreg collection, DO11.10/RAG2 KO/eFox mice were immunized with OVA (200 μg/head, s.c.) and treated with AS (30 mg/kg,

p.o.). After 1 week post-treatment, Foxp3$^+$ cells were collected by FACSAriaII. Cells were lysed in RLT buffer (Qiagen) containing 1% 2-Mercaptoethanol, followed by RNA reverse transcription by SMART-seq v4 Ultra Low Input RNA Kit for Sequencing (Clontech). Before preparation of the cDNA library by using Kapa Library preparation kit (KAPA), cDNA samples were fragmented by Covaris Focused-ultrasonicator S220.

Sequence of the cDNA libraries were analyzed by Ion-proton (Thermo Scientific). Acquired sequencing results were mapped to the reference genome information (mm9, provided by UCSC) using Tophat2 and unmapped sequences were analyzed again by bowtie2. Normalized FPKM values were provided by Cuffnorm of Cufflinks package (version 2.2.1, Trapnell Lab). To analyze differentially expressed genes (DEG) in each comparison, raw tag count data were generated from mapped reads by using featureCounts in Subread packages (version 1.5.0-p3, Walter+Elisa Hall, ref. (*48*)). Normalized tag count value and false discovery rate were calculated using DESeq2 package in R (version 3.2.2). Genes of FDR > 0.25 in each comparison were assigned to the group of DEG.

In situ proximity ligation assay (PLA)

In situ PLA was performed with Duolink PLA probes and reagents (Sigma-Aldrich). Cultured cells were fixed for 10 min with 4% paraformaldehyde in phosphate-buffered saline (PBS), permeabilized for 15 min with 0.3% Triton X-100 in PBS, incubated with 1% BSA in PBS for 45 min and then with primary antibodies (rabbit polyclonal anti CDK8 Ab and mouse monoclonal anti STAT5 Ab) overnight at 4°C. After incubation with the primary antibodies, the cells were incubated with the PLA probes (secondary antibodies against two different species bound to two oligonucleotides: anti-mouse MINUS and anti-rabbit PLUS). Annealing of the PLUS and MINUS PLA probes occurs when CDK8 and STAT5 are in close proximity, and repeat sequences in the annealed oligonucleotide complexes are amplified and then recognized by a fluorescently labeled oligonucleotide probe. After the amplifying reaction, the cells were mounted with Duolink in situ mounting medium containing DAPI. PLA signals were obtained using LSM710 confocal microscope. z-Stacks were captured with sections spanning entire cells and images were presented as maximum intensity projection.

Immunofluorescence test

Cultured cells were fixed for 10 min with 4% paraformaldehyde in PBS and permeabilized for 15 min with 0.3% Triton X-100 in PBS. The cells were incubated with 1% BSA in PBS for 45 min and then incubated with the primary antibodies (rabbit polyclonal anti CDK8 Ab

(Thermo Fischer Scientific) and mouse monoclonal anti STAT5 Ab (Biolegend)) overnight at 4°C. After incubation with the primary antibodies, the cells were incubated with the secondary antibodies (Alexa Fluor 488-conjugated anti rabbit IgG (Thermo Fischer Scientific) and Alexa Fluor 594 conjugated anti mouse IgG (Thermo Fischer Scientific)) for 1 hour at room temperature. After incubation with Hoechst33342 in PBS, the cells were mounted with Prolong Diammond (Thermo Fischer Scientific). Confocal images were obtained using LSM710 confocal microscope.

Assay for transposase-accessible chromatin (ATAC)-seq.

ATAC-seq was performed as previously described (*24*). 1×10^6 naïve T cells were cultured in the 1 mL of 10% FCS-supplemented RPMI1640 medium, with the stimulation of 25 μL of Dynabeads Mouse T-Activator CD3/CD28, 50 U/mL (final concentration) of IL-2 and AS for 24 hours. ATAC peaks were visualized with IGV genome browser.

Chromatin immune-precipitation sequencing (ChIP-seq)

ChIP-seq analysis was performed basically according to the method described in ref. 23, with 1×10^6 naïve T cells cultured as described in the method for RNA-seq analysis.

ChIP: ChIP experiments used $5x10^5$ cells for each histone modification (H3K27ac, H3K27me3, H3K4me1, H3K4me3, H3K9me3), $1x10^7$ cells for Stat5, and $5x10^6$ cells for CDK8. Chromatin protein-DNA interaction was fixed by 1% formaldehyde for 5 min (Histone modification: H3K27ac, H3K27me3, H3K4me1, H3K4me3, H3K9me3) or 30 min (DNA-binding proteins; STAT5, CDK8). The sonication-fragmented lysate was incubated with Dynabeads IgG magnetic beads (Thermo Fischer Scientific) pre-coated with 2.5~5 μg of antibody, at 4°C for at least 6 hour. For reverse-crosslinking of precipitated-DNA-protein complex, DNA-protein solution was incubated with gently shaking at 65°C for precisely 24 hours. If needed, further fragmentation was performed using Covaris Focused-ultrasonicator S220.

Library preparation and Sequencing: genomic DNA library was prepared using KAPA library preparation Kit Ion Torrent (KAPA Biosystems), with the same protocol for cDNA library preparation in RNA-seq analysis, except the number of PCR cycles (histone modification; 11 cycles, DNA-binding proteins; 10 cycles), followed by DNA sequencing by IonS5 sequencing system (Thermo Fischer Scientific).

Bio-informative analysis: raw sequence fastq files were mapped to the reference mouse genome (mm9 provided by UCSC, 2007) by using Bowtie2.2.6 followed by calling ChIP peak region and defined differential/un-differential peak region using MACS2.

As for AS-enhanced STAT5 binding regions, annotating peak regions for the nearest TSS, tag coverage of given region, and motif enrichment analysis were performed using Homer2. In each defined peak region, the peak the center of which was within ± 1000 bases from the TSS site was classified as "Promoter-related modification" and the gene under that promoter was defined as "Promoter peak-related gene". For the definition of "Enhancer-related genes", TSS sites within ± 10000 bases from the H3K4me1 or H3K27ac peak regions were regarded as the genes under regulation of these histone modifications (H3K4me1 or H3K27ac peak areas within 3000 bases were treated as one broad peak region). After classifying peak regions and defining related genes, expression fold changes in AS-treated/non-treated were calculated from RNA-seq data (normalized tag counts) and shown as a cumulative histogram. Statistical significance was determined by the Kolmogorov-Smirnov test.

Chromatin Immuno-precipitation (ChIP) Assay

Mouse $CD4^+$ T cells were stimulated by plate-bound anti-CD3/CD28 and TGF-β (5 ng/mL), and cultured with DMSO or 1000 nM AS for 22 hours. The cells were subjected to ChIP assay with SimpleChIP Enzymatic Chromatin IP Kit (Cell Signaling Technology) according to the manufacturer's instructions with the use of phospho-STAT5 (Tyr694) antibody and rabbit isotype control antibody. The ChIP primer sequences used are as follows: Core promoter Forward: F: CTCACTCAGAGACTCGCAGCA; Core promoter Reverse: GCAAGCATGCATATGATCACC; CNS2 Forward: TACAGGATAGACTAGCCACTT; CNS2 Reverse: AATATGTTTTCCTATCGGGGT. Relative enrichment was calculated as a ratio to input chromatin.

Kinase assay

To evaluate compounds and calculate their IC50, CDK8 and CDK19 kinase assays were performed with QSS Assist CDK8/CycC_ELISA Kit and QSS Assist CDK19/CycC_ELISA Kit (Carna Biosciences) according to the manufacturer's instructions. GSK3α and GSK3β kinase assays were performed with GSK3α, GSK3β (Carna Biosciences) and Z-Lyte Kinase assay kit-ser/thr9 peptide (Thermo Fisher Scientific) according to the manufacturer's

instructions. Kinase inhibition IC50 is defined as the concentration of inhibitor that reduces phosphorylation by half compared to DMSO control.

For the evaluation of STAT5b phosphorylation by CDK8, GST-STAT5b was purified with Glutathione Sepharose 4B (GE healthcare) from BL21 lysates transfected with pGEX 6P-1 (GE healthcare) harboring STAT5b (709-786 a.a.) subcloned from pCMV6-STAT5b. 293T cells were transfected with pCMV6-CDK8 (wild type or kinase-dead), pCMV-CyclinC (Origene, RC220544), pCMV6-MED13 (Origene, MR224038) and pF4K-CMV harboring MED12 subcloned from pF1K-MED12 (Promega, FXC12080). CDK8 submodules were pull-downed with Anti-FLAG(R) M2 Magnetic Beads (Sigma) from the 293T lysates. The purified kinases were incubated with 10 ng GST-STAT5b in kinase assay buffer (5 mM Tris-HCl (pH7.5), 10 mM MgCl2, 2 mM DTT, 100 mM KCl, 0.01% Brij35, 100 μM ATP). The reaction products were subjected to immunoblotting with anti-phospho-Stat5b (S731).

Kinase selectivity profiles of compounds were evaluated by biochemical assays with a panel of recombinant kinases at Carna Biosciences. Compounds were assayed at 100 nM (duplicate). Assay formats included IMAP assays and off-chip mobility shift assays. ATP concentrations were set near Km values. Data are expressed as percent inhibition of the kinase activity compared to DMSO control.

Determination of drug concentration in the peripheral blood

BALB/c mice were orally administered with 3, 10 or 30 mg/kg AS. Plasma samples were collected from mice at 1, 2, 4, 8 and 24 hours after administration to measure drug levels using HPLC-tandem mass spectrometry.

OVA immunization

DO11.10 mice were immunized subcutaneously with 100 μL of an emulsion containing 200 μg of OVA (323-339) in 50 μl of PBS and 50 μL of complete Freund's adjuvant (CFA). AS was administrated (30 mg/kg, p.o.) for 7 days, and draining lymph nodes were collected for flow cytometry analysis, bisulfite sequencing analysis and RNA-sequencing analysis.

Adoptive transfer of retrovirus- infected $CD4^+$ T cells

Naive $CD4^+$ T cells were isolated from DO11.10$Rag2^{-/-}$Foxp3-eGFP reporter mice. The cells were stimulated with anti-CD3/CD28 mAbs for 22 hours, and infected with retroviruses and incubated for 22 hours in the absence of IL-2. For this experiment, truncated LNGFR, instead

of eGFP, was inserted into a retroviral plasmid as a marker of infection. Then cells were rested for 10 days in the presence of 100 U/mL IL-2 until cell transfer into mice. BALB/c-nu/nu mice were transferred with the retrovirus-infected cells on day 0, and treated with IL-2/anti-IL-2 Ab complexes on day 7, and then immunized with 100 μg of OVA emulsified with complete Freund's adjuvant at the base of the tail on day 14. Inguinal lymph node cells were collected from the mice and examined by flow cytometry on day 20.

DNFB-induced contact hypersensitivity (CHS)

Mice were sensitized epicutaneously at day 0 and 7 by applying 100 μL of 0.5 % DNFB diluted in acetone on the abdominal skin and challenged at day 14 by applying 20 μL 0.5 % DNFB on the ear. In order to deplete Treg, FDG mice were treated with 1000 ng diphtheria toxin (daily, i.p.) from days 0 to 14.

Experimental autoimmune encephalomyelitis (EAE)

Mice were immunized subcutaneously with 100 μL of an emulsion containing 100 μg of MOG peptide in 50 μL of PBS and 50μL of CFA on day 0. CFA was prepared by mixing incomplete Freund's adjuvant (Difco) with 20 mg/ml of Mycobacterium tuberculosis H37RA (Difco). Pertussis toxin (List Biological Laboratories Inc., Campbell, CA) was injected on days 0 and 2 (100 ng/mouse, i.p.). Clinical scoring was performed according to the following scale: 0, no clinical signs of EAE; 1, tail weakness or tail paralysis; 2, hind leg paraparesis or hemiparesis; 3, hind leg paralysis or hemiparalysis; 4, tetraplegia or moribund; and 5, death. Statistical analysis was performed according to previous discussion (*49*). Histological analysis was carried out by using Luxol Fast Blue Stain Kit (ScyTec Laboratories, Inc.).

Non-obese diabetic (NOD)

In this study, 8 weeks old female NOD mice were prepared and maintained with tap-water. The incidence of diabetes was determined by monitoring blood glucose levels. Histological analysis was performed by using pancreas from 10 weeks old mice. Insulitis scoring was performed according to the following scale: 0, no insulitis; 1, peri-insulitis and insulitis involving less than 25 % islet; 2, more than 25 % islet; and 3, more than 75 % islet infiltration.

Delayed-type hypersensitivity (DTH) induction and assessment

Eight-week-old female BALB/c mice were immunized subcutaneously with 50 μg of ovalbumin (OVA) (SIGMA) emulsified with complete Freund's adjuvant (CFA) (Difco) in both hind footpads. Seven days after immunization, the mice were challenged with the intradermal injection of 20 μL of OVA (1 mg/mL in PBS) in the left ear. AS and dexamethasone were orally administered once a day during whole experimental period. The vehicle for both compounds was 0.5 % methylcellulose solution (MC). DTH was assessed by measuring the thickness of the ear before and 24 hours after the challenge by a micrometer (TECLOCK). Mice were sacrificed, and single-cell suspensions of auricular lymph nodes were prepared. The cells were then stained with PE-Cy7-labeled anti-MouseCD4, FITC-labeled anti-Mouse CD25, PerCP-Cy5.5-labeled anti Mouse KLRG1 and APC-labeled anti-Mouse Foxp3 and were assessed by flow cytometry.

BMDC culture

Bone marrow-derived dendritic cells (BMDCs) were generated in vitro as described (*50*). Briefly, the bone marrow cells were cultured in culture medium containing mouse granulocyte-macrophage colony-stimulating factor (20 ng/ml) for 8-10 days. These DCs were stimulated with LPS (0.1 μg/ml) or AS (1 μM) for 24 h.

Statistics

Values were expressed as means ± SD. Statistical significance was assessed by Student's t test (two groups), Kaplan Meier log-rank test (disease incidence) or non-repeated-measures analysis of variance (ANOVA) followed by the Bonferroni test (versus control), Dunnett's test or SNK test (multiple comparisons). A probability of less than 5% ($P< 0.05$) was considered statistically significant.

Supplemental References

41. R. Setoguchi, S. Hori, T. Takahashi, S. Sakaguchi, Homeostatic maintenance of natural Foxp3(+) CD25(+) CD4(+) regulatory T cells by interleukin (IL)-2 and induction of autoimmune disease by IL-2 neutralization. *J Exp Med* **201**, 723-735 (2005).
42. J. M. Kim, J. P. Rasmussen, A. Y. Rudensky, Regulatory T cells prevent catastrophic autoimmunity throughout the lifespan of mice. *Nat Immunol* **8**, 191-197 (2007).
43. Y. Ito, M. Hashimoto, K. Hirota, N. Ohkura, H. Morikawa, H. Nishikawa, A. Tanaka, M. Furu, H. Ito, T. Fujii, T. Nomura, S. Yamazaki, A. Morita, D.A. Vignali, J.W. Kappler, S. Matsuda, T. Mimori, N. Sakaguchi, S. Sakaguchi, Detection of T cell responses to a ubiquitous cellular protein in autoimmune disease. *Science* **346**, 363-368 (2014).
44. A. Sugimoto, R. Kawakami, N. Mikami, Transcription Factors Downstream of IL-4 and TGF-β Signals: Analysis by Quantitative PCR, Western Blot, and Flow Cytometry. *Methods Mol Biol* **1585**, 141-153 (2017).
45. M. O. Gold, J. P. Tassan, E. A. Nigg, A. P. Rice, C. H. Herrmann, Viral transactivators E1A and VP16 interact with a large complex that is associated with CTD kinase activity and contains CDK8. *Nucleic Acids Res* **24**, 3771-3777 (1996).
46. S. Akoulitchev, S. Chuikov, D. Reinberg, TFIIH is negatively regulated by cdk8-containing mediator complexes. *Nature* **407**, 102-106 (2000).
47. F. A. Ran, P.D. Hsu, J. Wright, V. Agarwala, D.A. Scott, F. Zhang, Genome engineering using the CRISPR-Cas9 system. *Nat Protoc* **8**, 2281-2308 (2013).
48. Y. Liao, G. K. Smyth, W. Shi, featureCounts: an efficient general purpose program for assigning sequence reads to genomic features. *Bioinformatics* **30**, 923-930 (2014).
49. K. K. Fleming, J.A. Bovaird, M.C. Mosier, M.R. Emerson, S.M. LeVine, J.G. Marquis, Statistical analysis of data from studies on experimental autoimmune encephalomyelitis. *J Neuroimmunol* **170**, 71-84 (2005).
50. N. Mikami, K. Sueda, Y. Ogitani, I. Otani, M. Takatsuji, Y. Wada, K. Watanabe, R. Yoshikawa, S. Nishioka, N. Hashimoto, Y. Miyagi, S. Fukada, H. Yamamoto, K. Tsujikawa, Calcitonin gene-related peptide regulates type IV hypersensitivity through dendritic cell functions. *PLoS One* **9**, e86367 (2014).

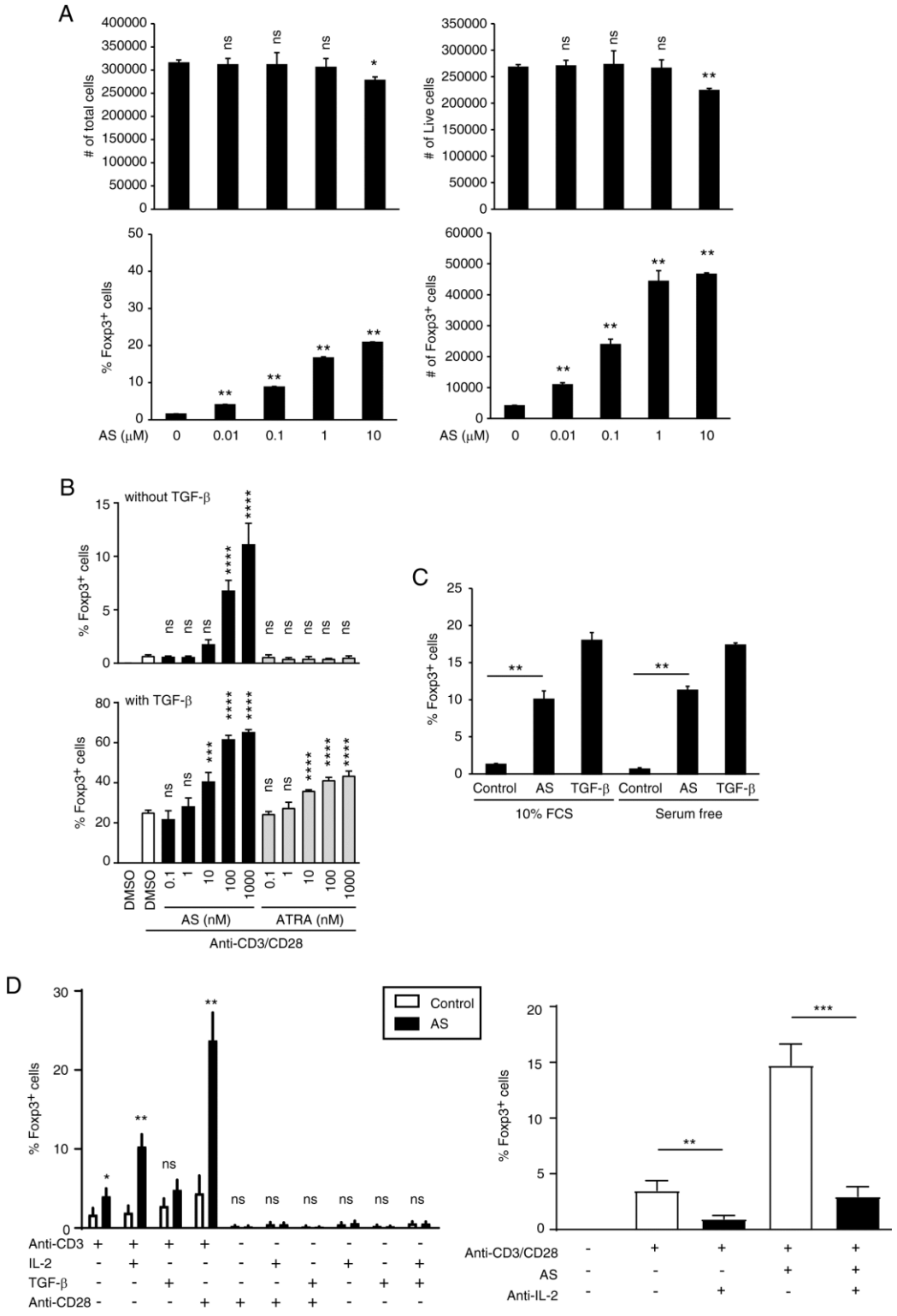

Fig. S1. AS dose, TGF-β and IL-2 in AS-dependent *in vitro* induction of Foxp3$^+$ T cells. **(A)** Mouse naïve CD4$^+$ cells were incubated with indicated concentrations of either AS and analyzed the survival, cell number and Foxp3 expression by flow cytometry (n=3). **(B)** Mouse naive Th cells were incubated with indicated concentrations of either AS or ATRA

under stimulation with anti-CD3/CD28 mAb in the absence or presence of TGF-β for 44 hours, and examined for expression of Foxp3 in live $CD4^+$ cells by flow cytometry (n=3). (**C**) Mouse naïve Th cells were stimulated under serum-free condition (n=3). (**D**) Mouse naive $CD4^+$ T cells were incubated with indicated stimuli for 44 hours in the absence or presence of 1000 nM AS2863619, IL-2 or anti-IL-2 mAb, and expression of Foxp3 in live $CD4^+$ cells was assessed by flow cytometry (n=3). Values indicate means+SD. *P<0.05, **P<0.01, ***P<0.001, ****P<0.0001 (Dunnett's test in **A**, SNK method in **B and C,** and unpaired t-test in **D**). ns, not significant.

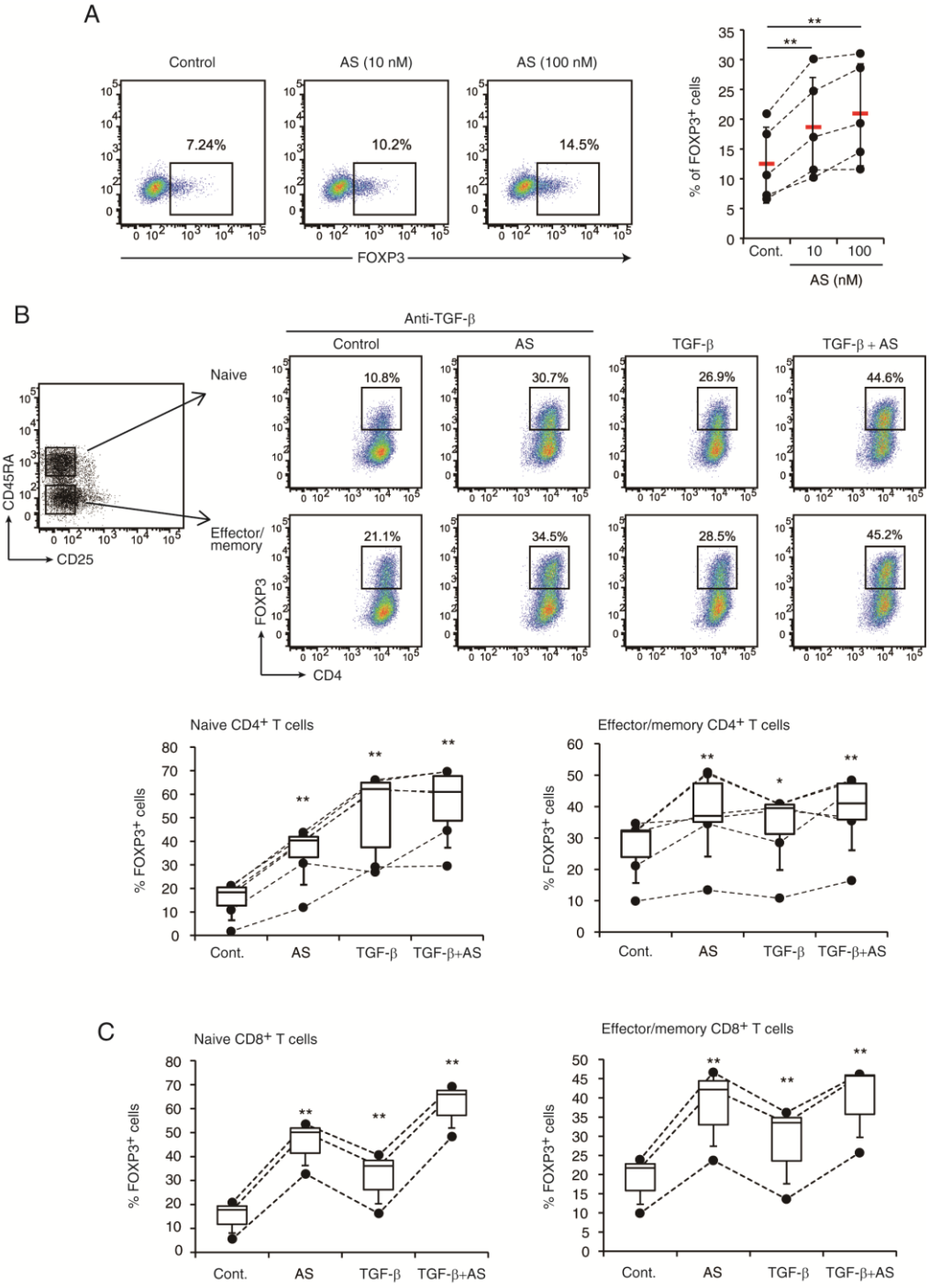

Fig. S2. ***In vitro*** **induction of FOXP3 in human Tconv cells by AS.** (**A**) Induction of FOXP3$^+$ cells in human naïve CD4$^+$ cells. Human PBMC-derived naïve CD4$^+$ T cells were anti-CD3/ CD28 stimulated in the presence of AS (n=5). (**B and C**) Naïve or effector/memory human CD4$^+$ T cells (**B**, n=6) and CD8$^+$ T cells (**C,** n=3) were stimulated with 100 nM AS or TGF-β. Vertical bars indicate means ± SD. $^{**}P < 0.01$, $^{*}P < 0.05$ (SNK method).

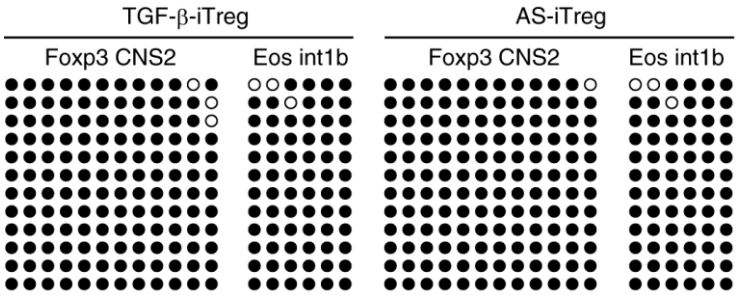

Fig. S3. Inability of AS to induce Treg-specific DNA hypomethylation *in vitro* in Tonv cells. Bisulfite sequencing showing Treg-specific demethylated regions at Foxp3 CNS2 and Eos int1b in TGF-β-induced and AS-induced iTreg cells. Representative of 2~4 experiments.

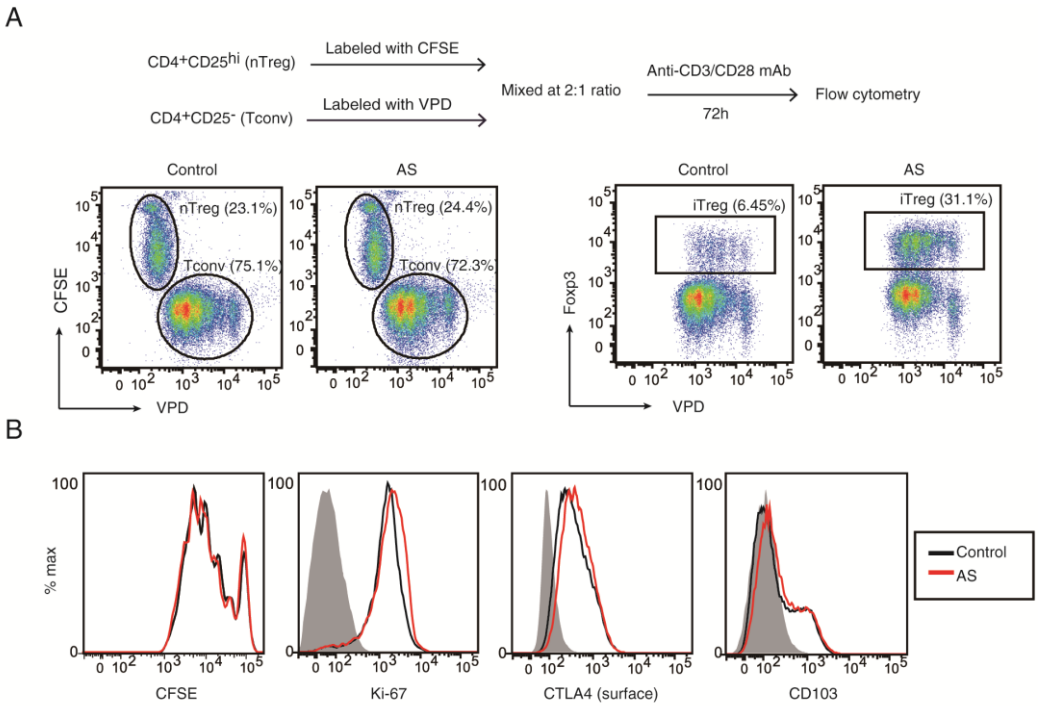

Fig. S4. ***In vitro*** **effects of AS on the proliferative activity and the phenotype of nTreg cells.** (**A**) Method of mixed culture of nTreg (CFSE-labeled) and Tconv cells (VPD-labeled). Mixed cells were stimulated with anti-CD3/ CD28 dynabeads for 72 hours. (**B**) Proliferation and expression of Foxp3 and other Treg signature molecules were analyzed by flow cytometry after in vitro stimulation with or without AS. Representative of two independent experiments.

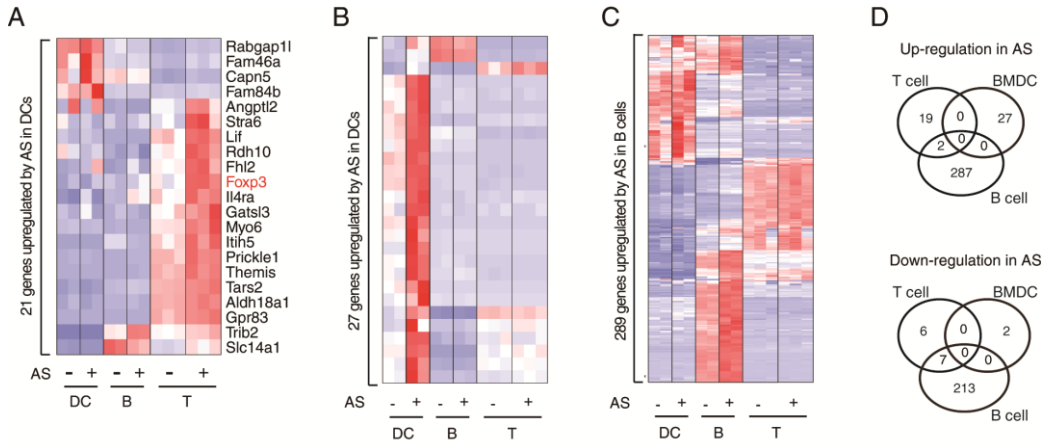

Fig. S5. Effects of AS on gene expression by T, B, and dendritic cells. (**A-C**) Heat map of T cell DEGs (**A**), B cell DEGs (**B**) and BMDC DEGs (**C**) in T cell (n=3), B cell (n=2) and BMDC (n=2). Cells were cultured for 24 hours, AS-treated for last 6 hours, and analyzed by RNA-seq analysis. (**D**) Venn diagram of differentially expressed genes (DEGs) between stimulated T cells (n=3), B cells (n=2) and BMDC (n=2) in the presence or absence of AS. FDR < 0.25 in RNA-seq are defined as significant DEGs. The numbers of genes in each fraction are shown.

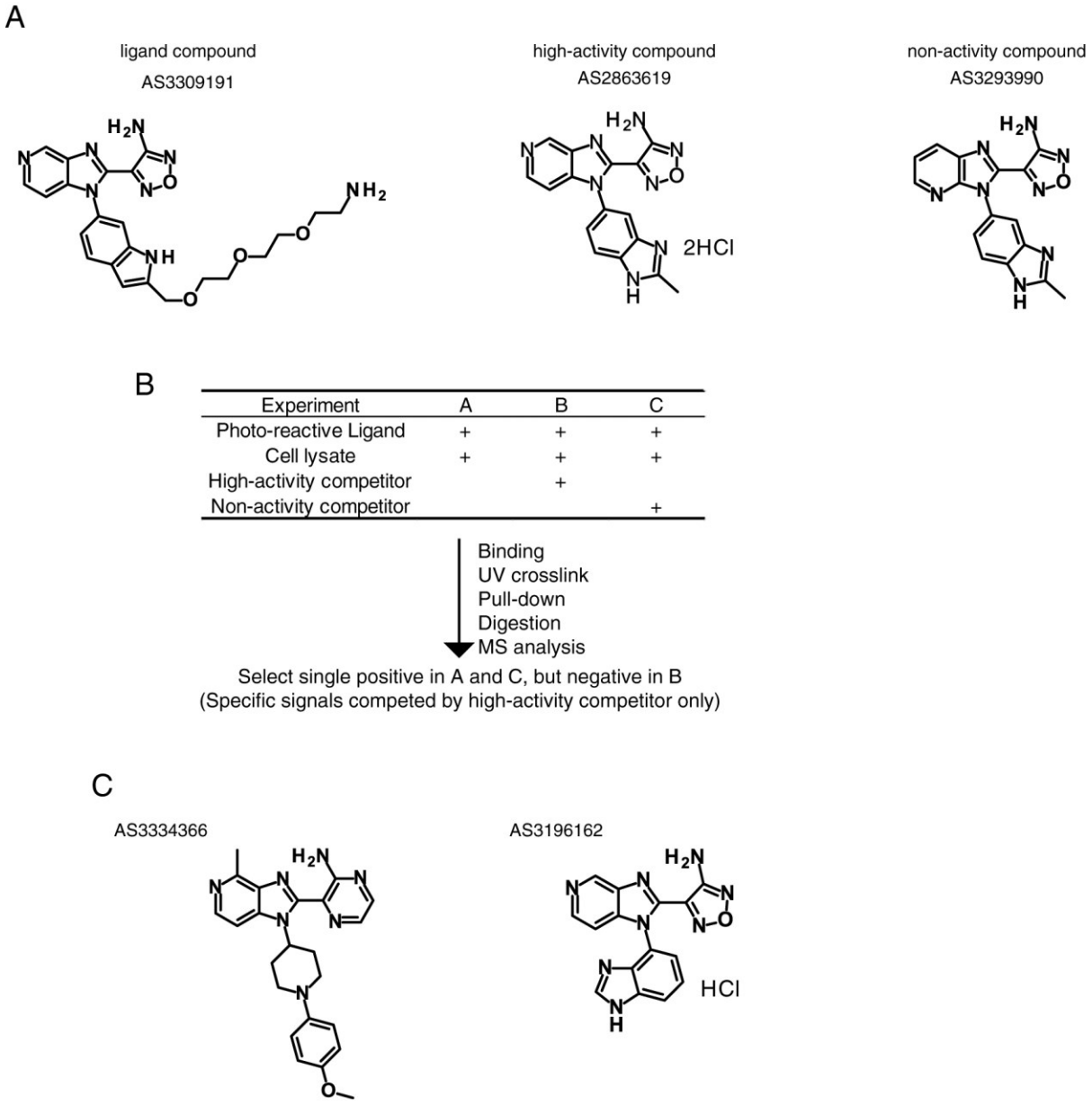

Fig. S6. Identification of AS targets by chemical proteomics. (**A**) Chemical structure of compounds used for affinity purification. AS3293990, an inactive AS analogue, was used as a non-competitive displacer in affinity purification. (**B**) Chemical proteomics workflow based on affinity purification followed by nano-liquid chromatography (LC) tandem mass spectrometry (MS/MS). The AS-specific candidates were extracted by removing ligand-binding molecules in the presence of AS. (**C**) Chemical structure of AS3334366 and AS3196162.

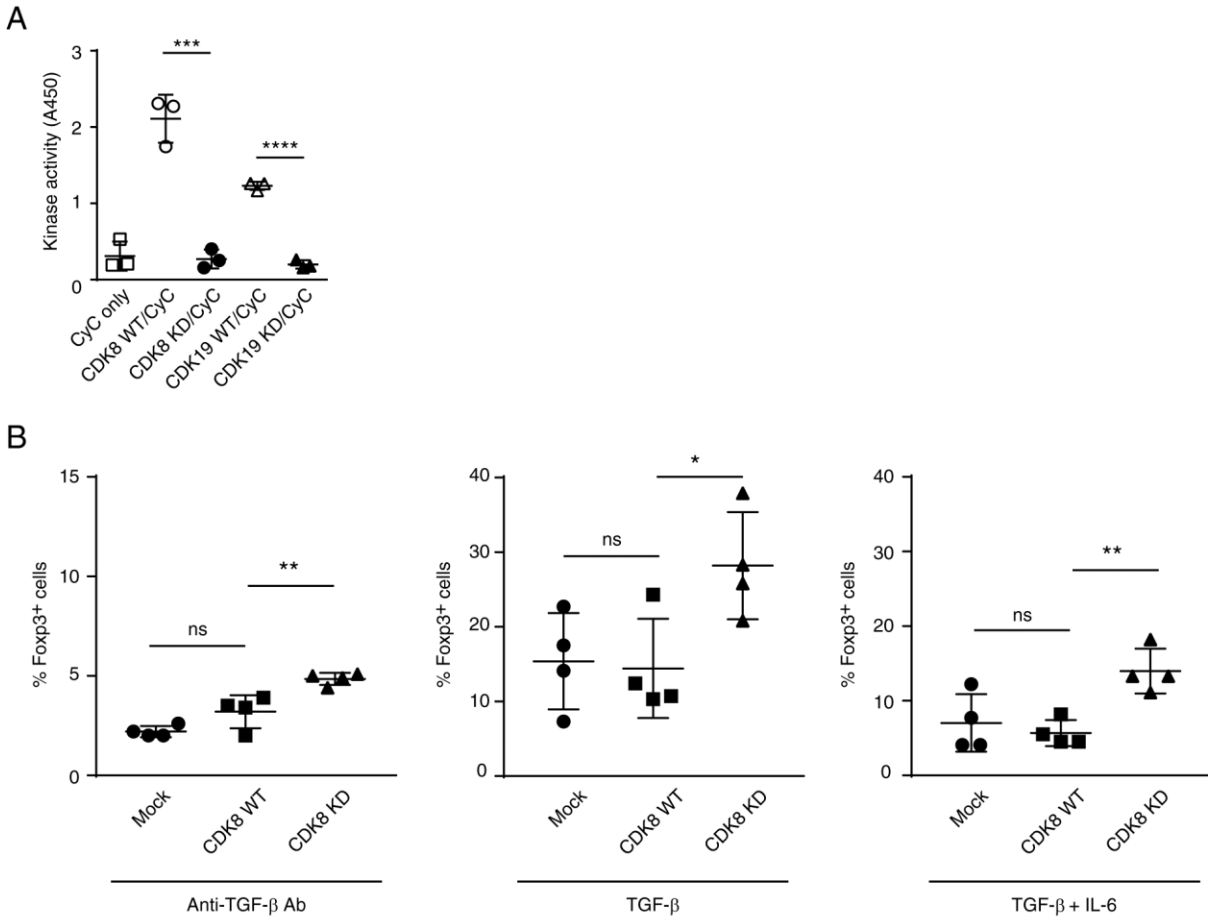

Fig. S7. Dominant-negative type impaired kinase activity of kinase-dead (KD) CDK8 or CDK19 and Foxp3 induction in CD4$^+$ T cells by their retroviral expression. (A) Impaired kinase activity by D173A CDK8 or D173A CDK19 expression. 293T cells were transfected with pCMV6 vectors encoding FLAG-tagged Cyclin C in combination with CDK8 wild type, CDK19 wild type, D173A CDK8 or D173A CDK19. Transfected cells were incubated for 2 days, and lysed for immuno-precipitation with anti- Flag conjugated magnet beads. The kinase activity of immuno-precipitates was assessed by Elisa-based kinase assay (n=3). **(B)** Effects of retroviral expression of WT or KD CDK8 on Foxp3$^+$ cell generation. Mouse CD4$^+$ T cells infected with retrovirus harboring GFP (mock control), WT or KD CDK8 were stimulated with anti-CD3/CD28 and IL-2 in the presence of indicated reagents. The percentages of Foxp3$^+$ cells among CD4$^+$ T cells were analyzed by flow cytometry (n=4). Vertical bars designate means ± SD. *P<0.05, **P<0.01, ***P<0.001, ****P<0.0001 (t-test).

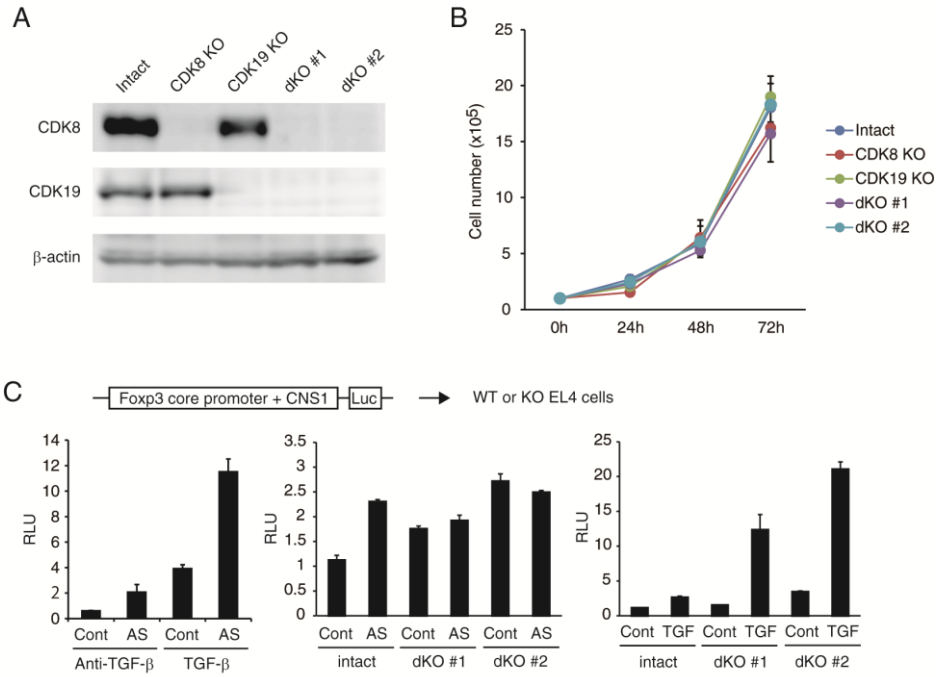

Fig. S8. Generation of CDK8/19 KO EL4 cell lines. (**A**) Western blot analysis of KO cells for CDK8 and CDK19 expression. Representative of two independent experiments. (**B**) Proliferation of KO cells was estimated by counting cell numbers (triplicate). (**C**) Luciferase assay using the EL4 cell lines and a Foxp3 reporter plasmid with the Foxp3 promoter+CNS1 (triplicate). Cells were anti-CD3/CD28 stimulated in the presence of AS after plasmid transfection. Vertical bars designate means ± SD.

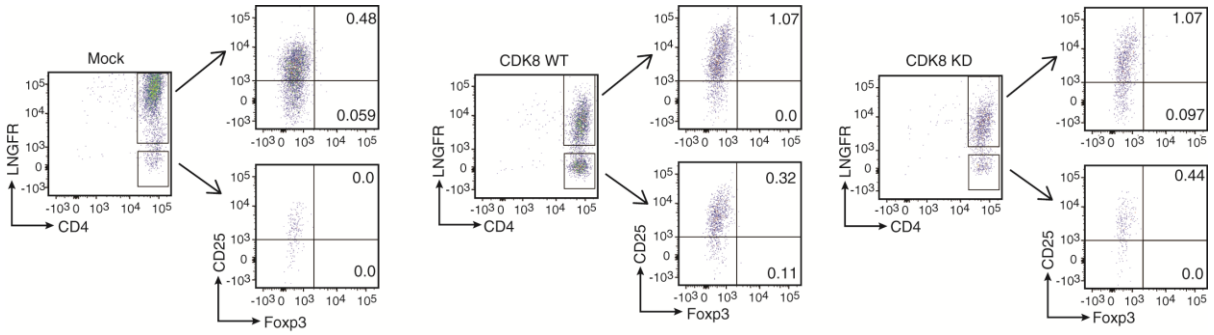

Fig. S9. Retroviral expression of kinase dead (KD) or WT CDK8 in CD4$^+$ T cells. Naive CD4$^+$ T cells isolated from DO11.10Rag2$^{-/-}$Foxp3-eGFP reporter mice were stimulated with anti-CD3/CD28 for 22 hours, infected with mock or CDK8-KD or -WT-carrying retroviruses, incubated for another 22 hours in the absence of IL-2, and rested for 10 days in the presence of 100 U/mL IL-2 until their transfer into BALB/c-nu/nu mice. The cells used for the transfer were analyzed by flow cytometry. LNGFR was used as a marker of infection. Representative of two independent experiments.

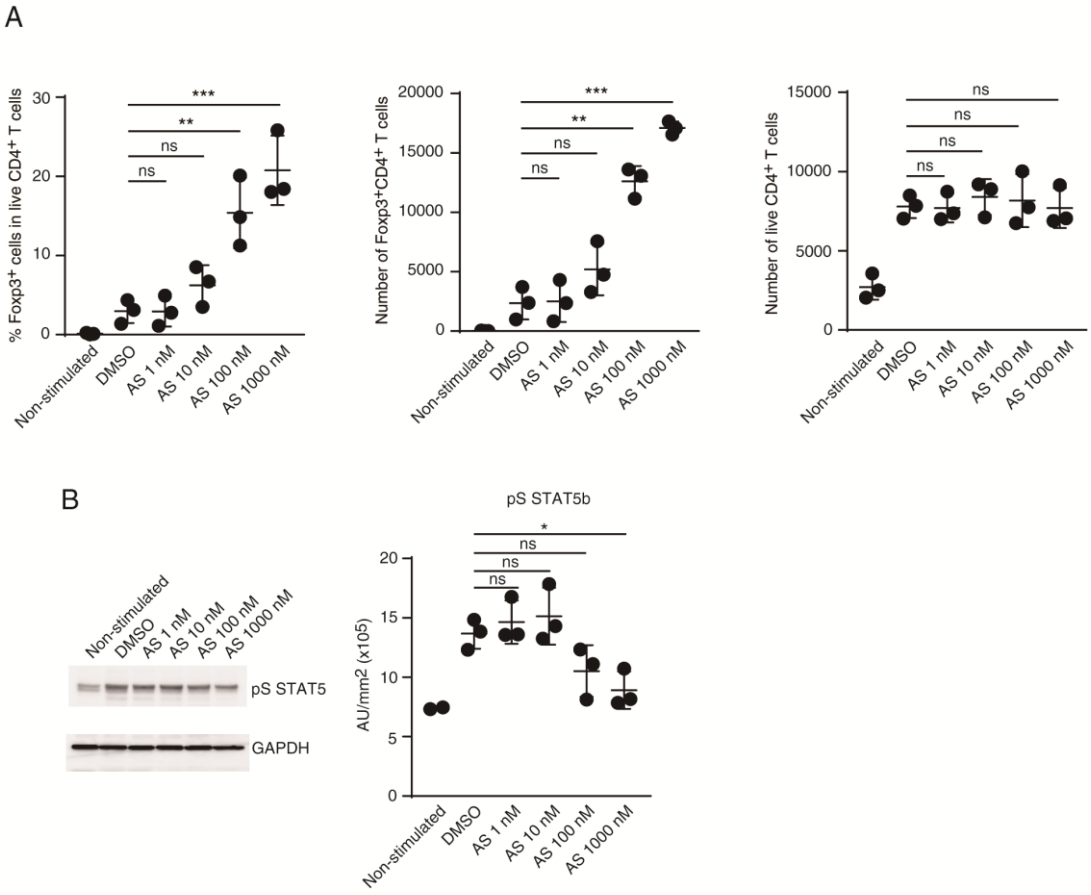

Fig. S10. Effects of AS on serine phosphorylation of STAT5. (**A, B**) Mouse $CD4^+$ T cells were stimulated with anti-CD3/CD28 for 22 hours, in the absence (DMSO) or presence of 1, 10, 100, or 1000 nM AS, and assessed for the percentage of $Foxp3^+$ cells among live $CD4^+$ T cells by flow cytometry (**A**), or subjected to immunoblotting for pS-STAT5b (**B**). Signal intensity was quantified and normalized by GAPDH (n=3). *P<0.05, **P<0.01, ***P<0.001(Dunnett's test). ns, not significant.

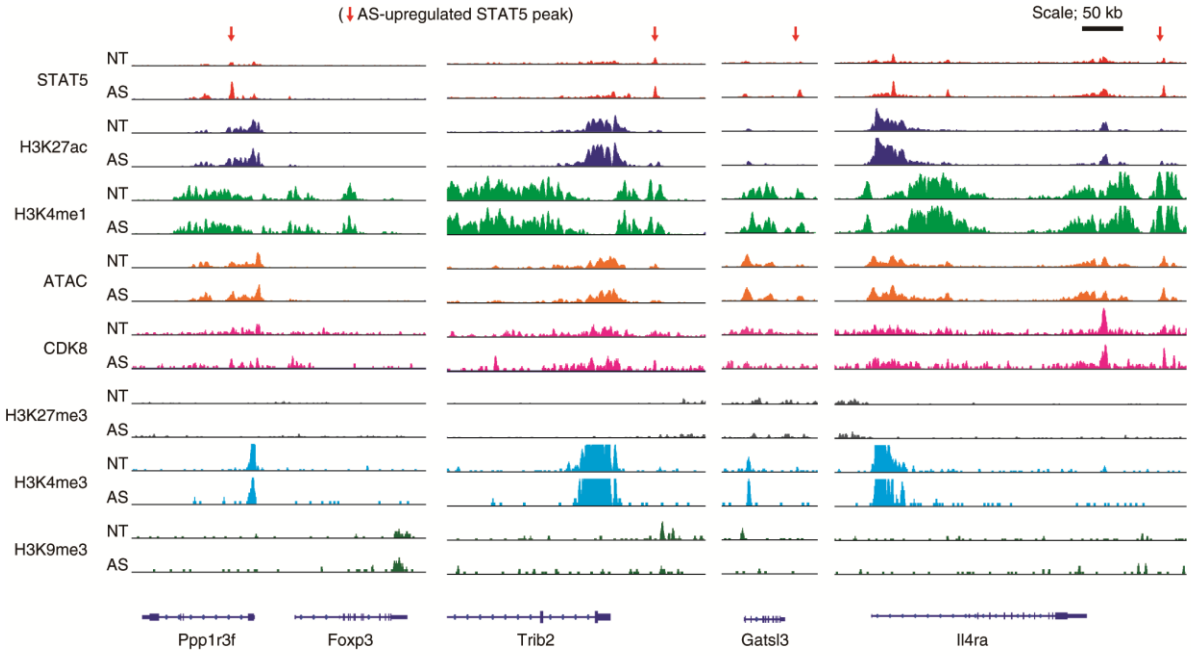

Fig. S11. Effects of AS on genome-wide STAT5 binding. ChIP-seq and ATAC-seq analysis between AS-treated (AS) and non-treated (NT) T cells. Cells were anti-CD3/CD28 stimulated for 24 hours and analyzed by ChIP-seq or ATAC-seq analysis. Total numbers of differential peaks are calculated by MACS2 bdgdiff. Red arrows indicate STAT5 binding peaks augmented by AS treatment.

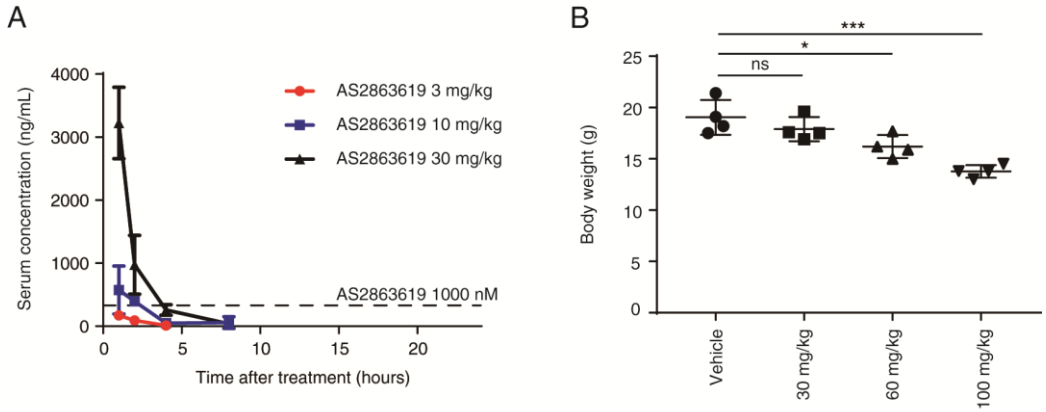

Fig. S12. Plasma concentration and body weight of mice treated with various doses of AS. (A) BALB/c mice were orally administered with 3, 10 or 30 mg/kg AS. Plasma samples were collected from mice at 1, 2, 4, 8 and 24 hours after administration to measure drug levels using HPLC-tandem mass spectrometry. Vertical bars designate means ± SD (n=3). The dotted horizontal line represents the concentration corresponding to 1 μM AS. **(B)** Mice were daily administered orally with indicated dose of AS. Body weight of the mice was assessed on day6. Vertical bars indicate means ± SD (n=4). **P < 0.001, *P < 0.05 (Dunnett's test, vs vehicle). ns, not significant.

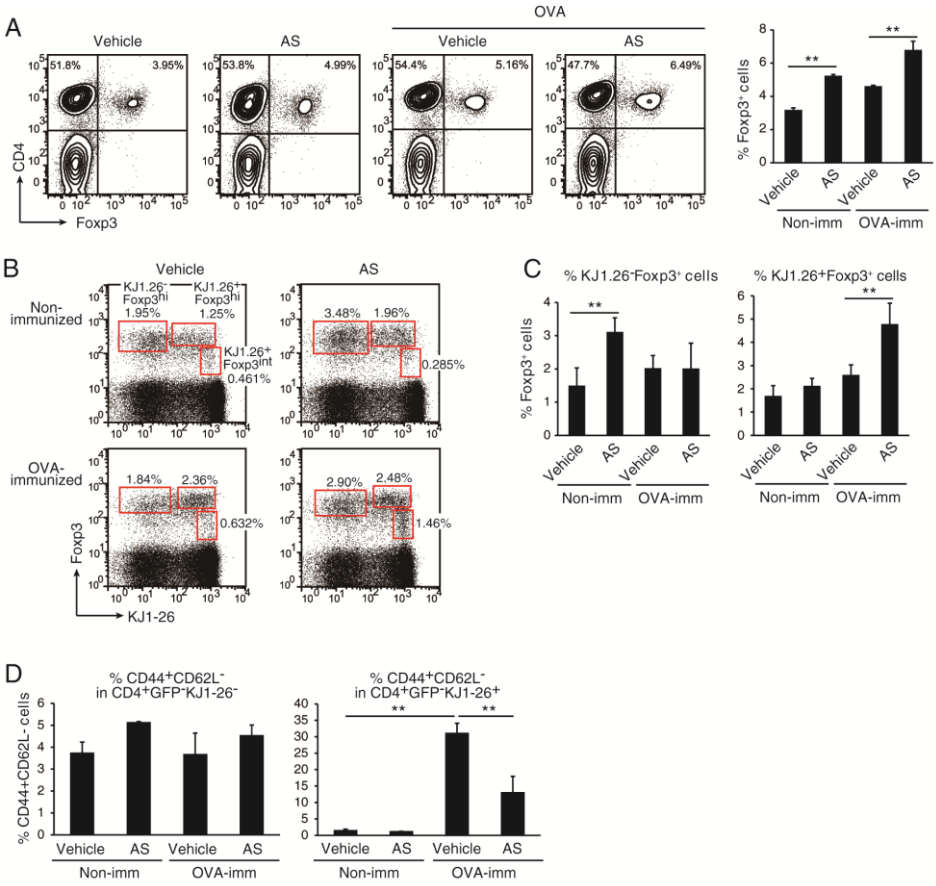

Fig.S13. Induction of pTreg cells by AS treatment and antigen immunization. (**A-D**) DO11.10/Foxp3-eGFP reporter mice were treated with 30 mg/kg AS every day for 7 days orally and subcutaneously immunized with OVA. CD4+ T cells in the draining lymph nodes of mice were stained for Foxp3, KJ1/26, CD44 and CD62L on day 8. Representative stainings and the percentages of whole Foxp3+ cells (**A**), KJ1-26^{+} or KJ1-26^{-} Foxp3^{+} cells (**B** and **C**), and KJ1.26^{+} or KJ1.26^{-} CD44^{+}CD62^{-}Foxp3^{-} cells (**D**) are shown. Vertical bars indicate means ± SD. **P < 0.01, (n=3, SNK method).

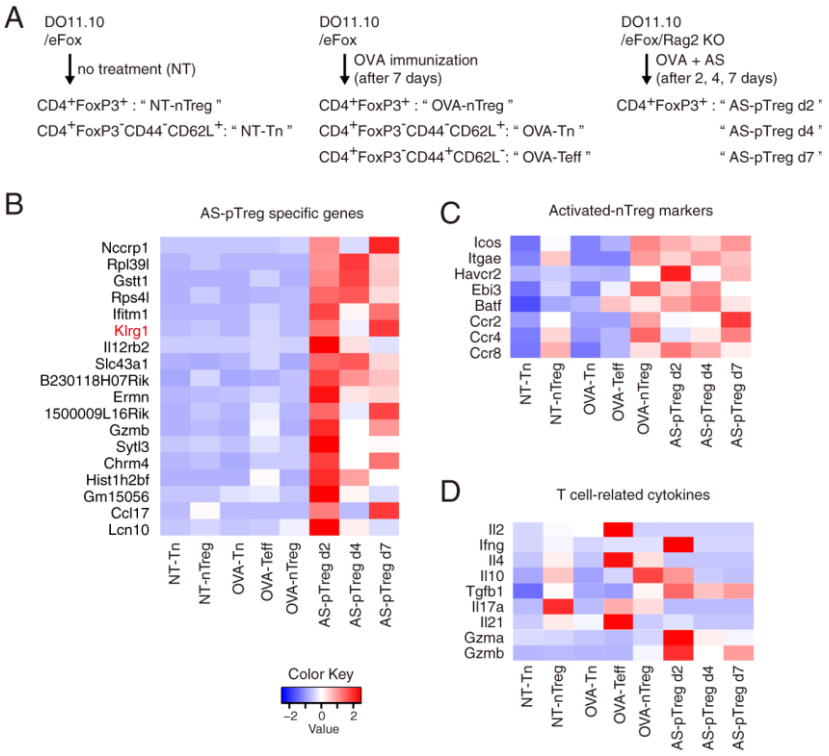

Fig. S14. RNA-seq analysis of AS-induced pTreg cells. (**A**) Experimental settings of RNA-seq analysis. DO11.10Rag2$^{-/-}$Foxp3-eGFP reporter mice were treated with OVA and AS, and Foxp3^{+} T cells from regional lymph nodes were collected as AS-pTreg. (**B**) Heat map showing z-score of the genes upregulated specifically in AS-induced pTreg cells by comparing AS-pTreg cells vs. other T cell populations. (**C**) Heat map showing z-score of activated-nTreg markers. (**D**) Heat map showing z-score of T cell cytokines.

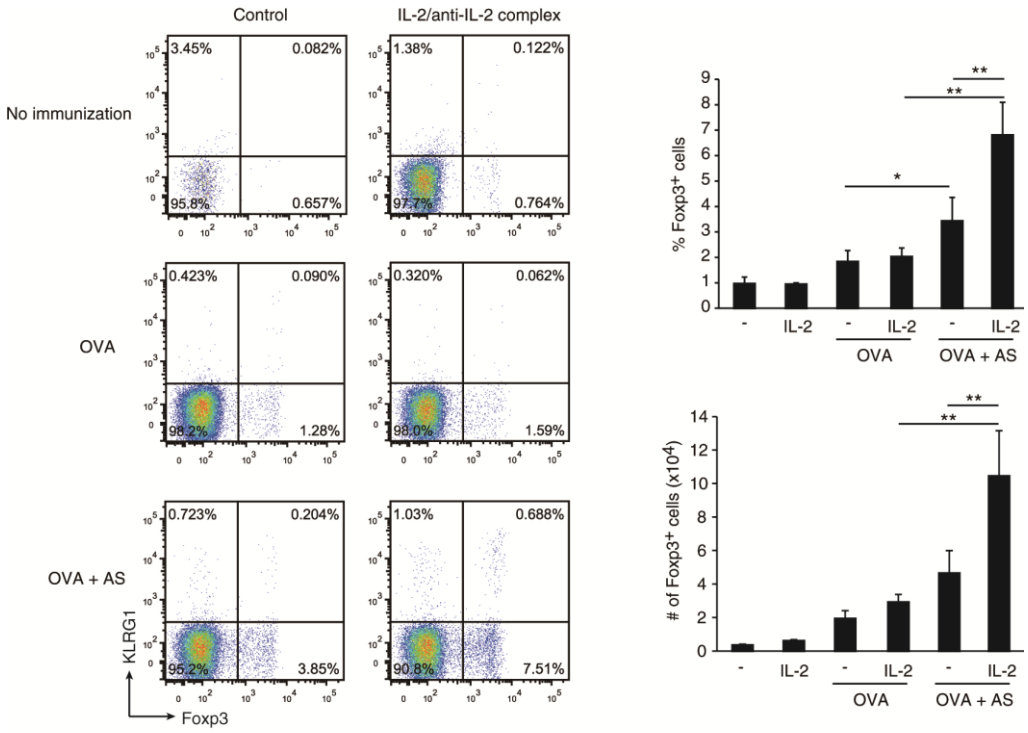

Fig.S15. IL-2 augments *in vivo* AS-mediated pTreg induction. DO11.10RAG2$^{-/-}$Foxp3-eGFP reporter mice were treated with AS (30 mg/kg every day for 7 days), immunized with OVA subcutaneously, and treated with IL-2/anti-IL-2 antibody treatment. CD4^{+} T cells in the draining lymph nodes of mice were stained for Foxp3 and KLRG1 on day 8. Representative staining (left panel) and the percentages and numbers of Foxp3^{+} cells among CD4^{+} T cells (n=3) (right panel). Vertical bars indicate means ± SD. $^{**}P < 0.01$, $^{*}P < 0.05$ (SNK method).

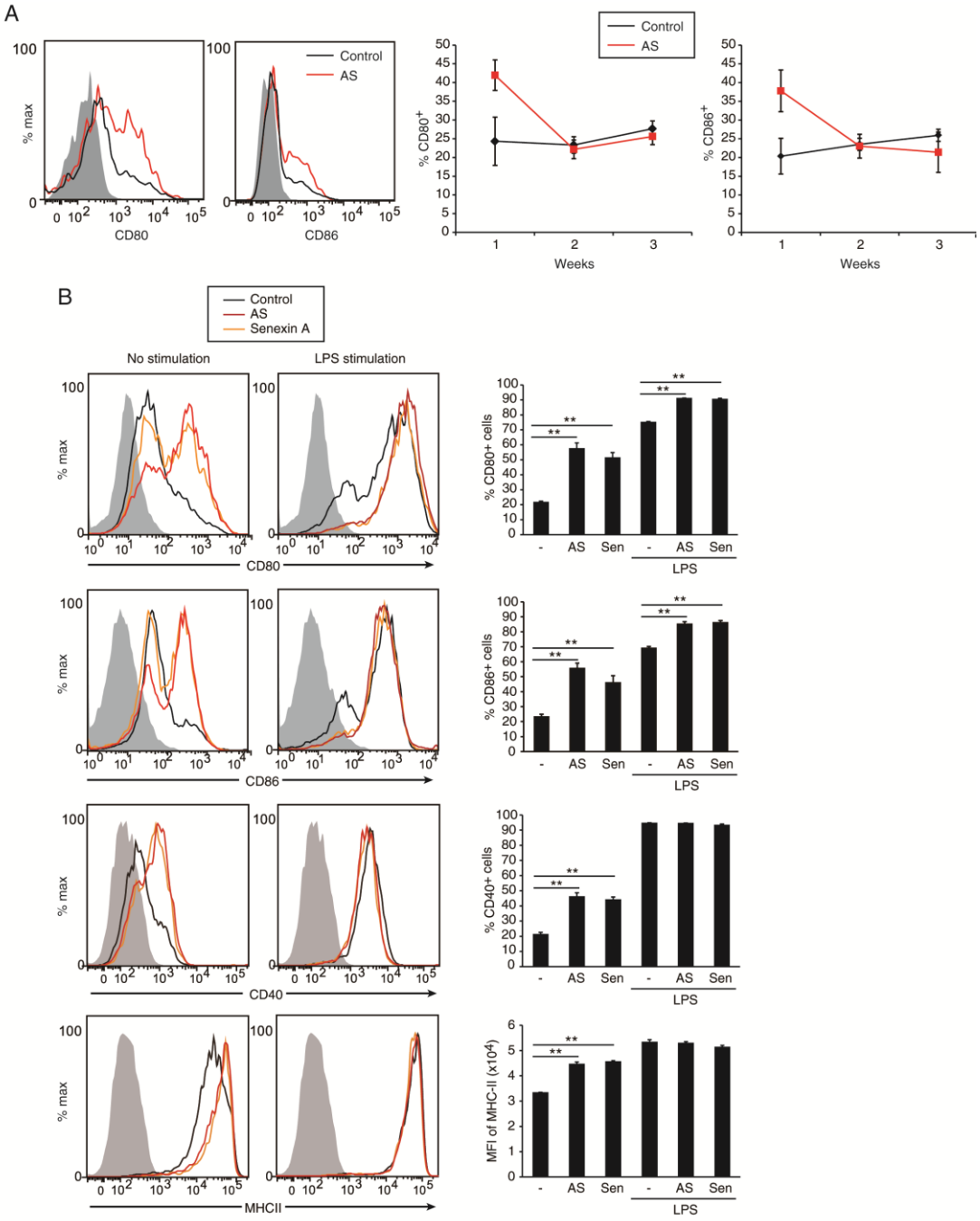

Fig. S16. Activation of dendritic cells by AS. (**A**) Induction of CD80 and CD86 in $CD11c^+$ cells of AS-treated non-immunized mice in vivo. Mice (n=3) were treated AS (30 mg/kg) without antigens for 7 days and $CD11c^+$ cells in peripheral lymph nodes were analyzed on day 8. (**B**) In vitro induction of CD80 and CD86 in BMDCs. BMDC were treated with 1.0 μM AS, Senexin A (Sen) and/or LPS for 24 hours, and examined for CD80, CD86, CD40, and MHC-II expression by flow cytometry (n=3). Vertical bars designate means ± SD. $^{**}P < 0.01$, $^{*}P < 0.05$ (SNK method).

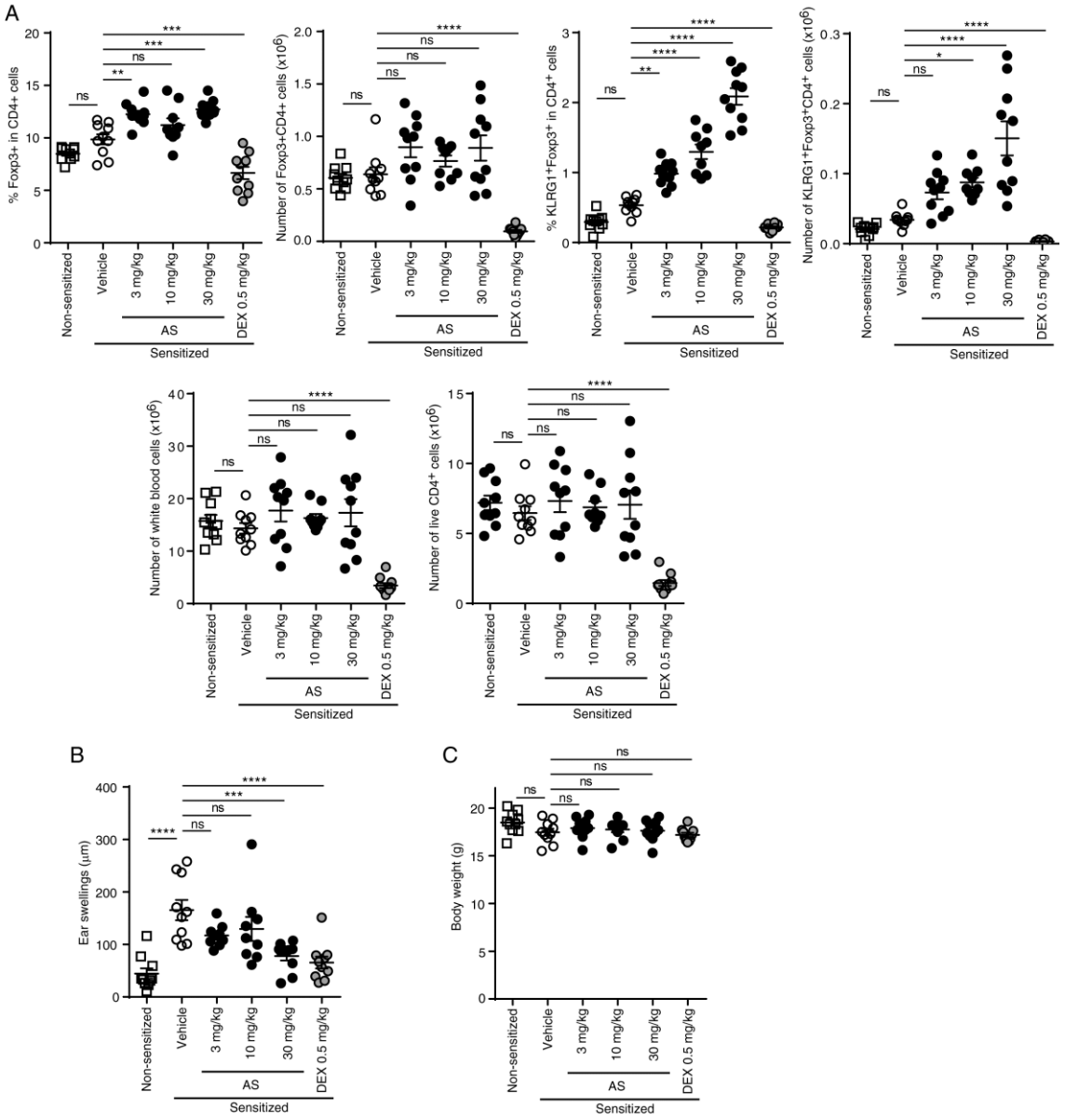

Fig. S17. Suppression of OVA-induced DTH by AS. (**A**) BALB/c mice were immunized subcutaneously with OVA emulsified with complete Freund's adjuvant in both hind footpads. Seven days after immunization, the mice were challenged with the intradermal OVA injection in the left ear. DTH was assessed by measuring the thickness of the ear before and 24 hours after the challenge. AS or dexamethasone (DEX) was orally administered once a day during whole experimental period. The percentages and numbers of $Foxp3^+$cells and $KLRG1^+Foxp3^+$cells among lymph node $CD4^+$ cells were analyzed by flow cytometry. The total number of whole white blood cells was counted by XT-2000i analyzer. (**B**) The degree of DTH was assessed by measuring ear thickness changes. (**C**) Body weight was measured on the last day of the DTH assessment. Vertical bars designate means ± SD; n=9 or 10 from two

independent experiments, *P<0.05, **P<0.01, ***P<0.001, ****P<0.0001 (Dunnett's test: vehicle vs AS, t test: vehicle vs dexamethasone).

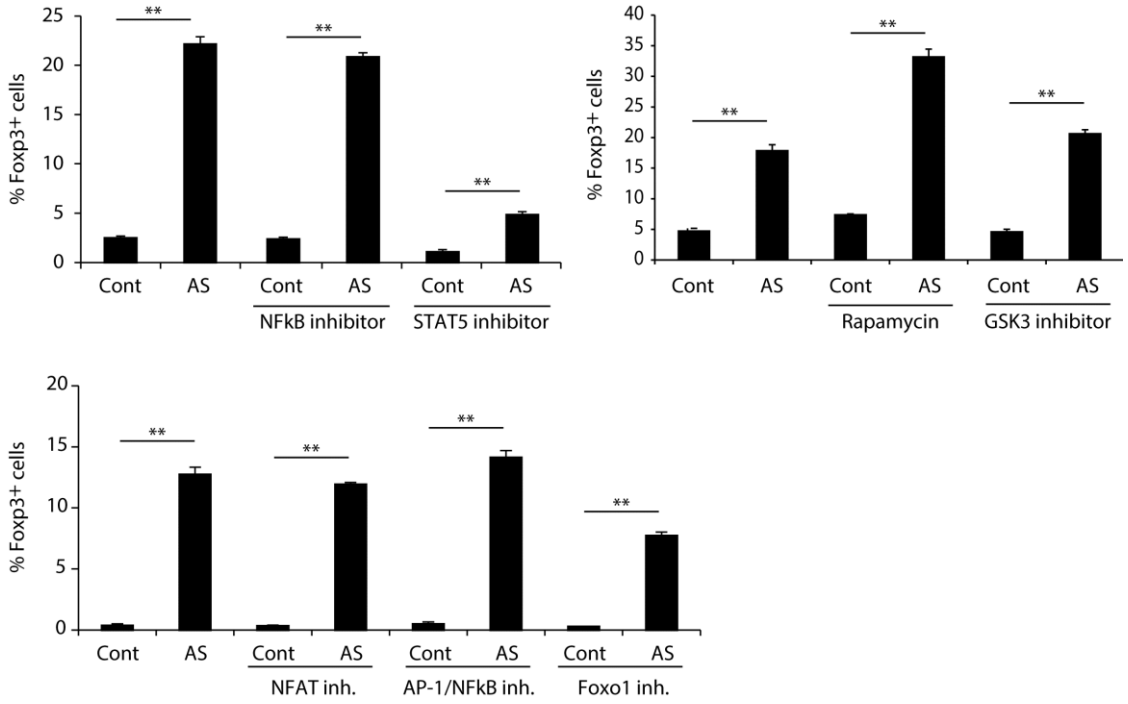

Fig. S18. *In vitro* Foxp3-inducing effects of AS in the presence of various inhibitors.

Mouse naïve $CD4^+$ cells were incubated with 1 μM of AS and other inhibitors (1 μM of BAY-11-7082, 10 μM of STAT5 inhibitor, 25 nM of rapamycin, 3 μM of GSK inhibitor, 20 μM of NFAT inhibitor, 100 nM of SP 100030 or 100 nM of Foxo1 inhibitor) in *in vitro* Foxp3 induction in Tconv cells as shown in Fig. 1. Foxp3 expression was analyzed by flow cytometry (n=3). Vertical bars designate means ± SD. $^{**}P < 0.01$ (SNK method).

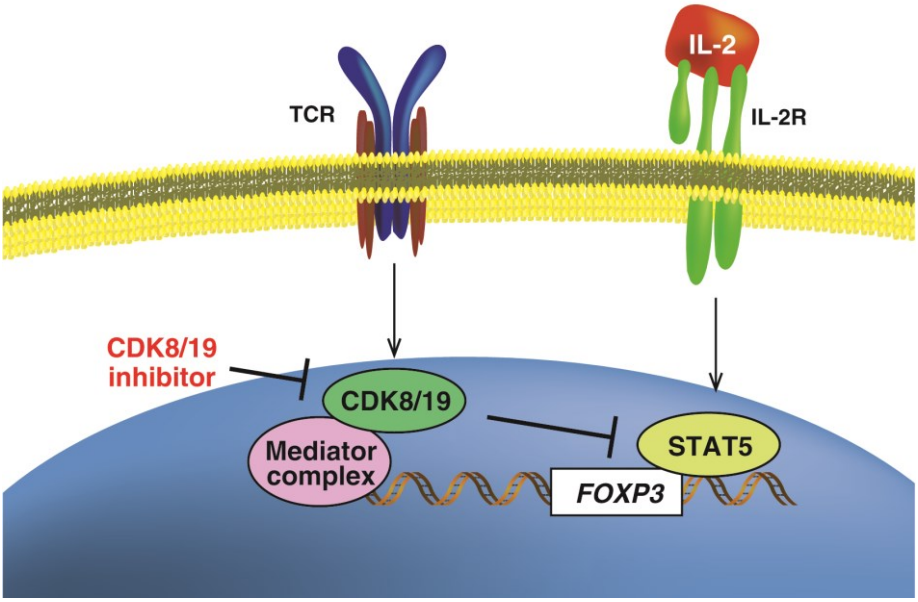

Fig. S19. Inhibition of STAT5 by CDK8/19 in activated Tconv cells and their Foxp3 expression induced by CDK8/19 inhibition via activating STAT5. See text.

Table S1. Kinase selectivity profiles of AS2863619 and AS3334366.

Kinase selectivity of AS2863619 and AS3334366 was evaluated by biochemical assays with a panel of recombinant kinases at 0.1 μM. Data are expressed as percent inhibition of the kinase activity compared to DMSO control (duplicate).

Kinase	% Inhibition		Kinase	% Inhibition		Kinase	% Inhibition	
	AS2863619 0.1 μM	AS3334366 0.1 μM		AS2863619 0.1 μM	AS3334366 0.1 μM		AS2863619 0.1 μM	AS3334366 0.1 μM
ABL	-2.9	-2.2	CRIK	14	5.2	p38 δ	1.2	-1.4
BTK	-12	-11.7	DAPK1	-6.5	-16.6	p70S6K	51.8	6.2
CSK	-1.6	-2.9	DCAMKL2	-2.2	-6.4	p70S6K β	5.6	-24.9
EGFR	-0.2	-2.7	DYRK1A	-1.9	17	PAK1	0.4	0.4
EPHA2	4.3	1.2	DYRK1B	5.4	8.9	PAK2	-3.4	-6.2
EPHB4	-4.1	-4.5	DYRK2	-1	-4.7	PAK4	-9.8	-0.5
FGFR1	-0.6	-2.6	DYRK3	-6.9	0.5	PAK5	-7.2	-3
FLT3	11.8	26.8	EEF2K	-11.8	-1.7	PAK6	-2.1	-1.9
IGF1R	1.1	0.9	Erk1	-1.3	0.7	PASK	-0.7	-5.2
ITK	-4.6	-6.6	Erk2	-4.2	-4.5	PBK	-10.7	-11.7
JAK3	2.9	3	Erk5	2	-0.1	PDHK2	0	0.5
KDR	11.9	16.7	GSK3 α	51.3	2.9	PDHK4	-12.1	-6.4
LCK	4.4	2.6	GSK3 β	52.7	-0.8	PEK	8	4.4
MET	-3.4	-2.2	Haspin	-0.5	12.5	PGK	1	1.2
PDGFR α	7.2	28.7	HGK	2.6	3.8	PHKG1	0.6	-2.2
PYK2	-0.8	-1.7	HIPK1	-7	-2.4	PHKG2	-0.2	-1.8
SRC	-6.2	-8.1	HIPK2	-5.7	0	PIM1	10.7	-4.8
SYK	-12.4	9.4	HIPK3	-6.6	-0.2	PIM2	-4.2	-1.6
TIE2	-1.6	-2.6	HIPK4	-6.4	-0.9	PIM3	-2.9	-1.4
TRKA	-1.9	-1.4	IKK α	3.1	7.3	PKAC α	0	0
TYRO3	-3.3	-1.9	IKK β	-6.1	-7	PKAC β	2.8	8.1
AKT1	-12.5	-12.8	IKK ε	-0.8	-0.6	PKAC γ	-4.4	-2.7
AKT2	-4	-2.8	IRAK1	-7.6	-12	PKC α	-7.3	-17.2
AKT3	-4.3	-2.1	IRAK4	-2.6	-2.2	PKC β 1	10	-14.5
AMPK α 1/ β 1/ γ 1	-6.3	-6.3	JNK1	-2.2	-1.5	PKC β 2	1.8	-5.9
AMPK α 2/ β 1/ γ 1	-0.2	-3.7	JNK2	0.4	0.4	PKC γ	-3.4	-7.5
AurA	1.6	0.1	JNK3	-4.2	-4.3	PKC δ	2.2	-0.4
AurA/ TPX2	-8.2	-1.9	LATS2	8.2	5.8	PKC ε	6.2	-9.7
AurB	-6.3	-4.2	LOK	-0.6	0.7	PKC ζ	-12.8	-8.3

AurC	-6.1	-2.8	MAP4K2	1	-1.9	PKC η	16.8	-8.7
BRSK1	-5.6	-9.7	MAPKAPK2	-9.5	-14.9	PKC θ	-3.3	-7.9
BRSK2	-2.7	-2.8	MAPKAPK3	-1.3	-3	PKC ι	3.8	-12.9
CaMK1 α	-2.5	-6.8	MAPKAPK5	-1.1	-4.3	PKD2	-12.4	-13.9
CaMK1 δ	1.1	-3.9	MARK1	-10.9	-9.9	PKD3	-0.1	-6.6
CaMK2 α	-5.9	-6.6	MARK2	-6.9	-7.5	PKN1	20.1	10.8
CaMK2 β	-4.3	8.5	MARK3	0.5	0.5	PKR	4.3	4.4
CaMK2 γ	-2.6	-5.7	MARK4	-9.5	1	PLK1	2.9	-2.1
CaMK2 δ	-0.9	-2.9	MELK	4.2	0.6	PLK2	1.8	10.1
CaMK4	-7.4	-7.2	MGC42105	-4.1	-8.7	PLK3	-5.9	-6.3
CDC2/CycB1	-2.5	-3.5	MINK	-4	-3.1	PRKX	-1.3	6.7
CDC7/ASK	1.8	-2.7	MNK1	-7	-5.4	QIK	0.8	11.3
CDK2/CycA2	-3.4	-2.3	MNK2	-12.3	2.4	ROCK1	22.7	-7.9
CDK2/CycE1	-11.3	-10.1	MRCK α	-2.5	-5.5	RSK1	63.6	-11.2
CDK3/CycE1	-4.7	-3.9	MRCK β	13.6	0.6	RSK2	70	-3.1
CDK4/CycD3	-20.1	-13	MSK1	39	15.9	RSK3	80.5	0.2
CDK5/p25	-7.4	-5	MSK2	-0.8	-3.6	RSK4	30.8	2
CDK6/CycD3	-5.7	-4.6	MSSK1	-17.7	-12.4	SGK	-2.4	-6.7
CDK7/CycH/MAT1	9.6	5.9	MST1	-1	-0.4	SGK2	2.2	-0.5
CDK9/CycT1	2.5	-0.3	MST2	-3.1	4.1	SGK3	-3.2	-5.4
CGK2	12.8	38.5	MST3	-2.8	-3.6	SIK	1.4	0.7
CHK1	2.8	-2	MST4	-4.8	-8.2	skMLCK	-5.6	-3.7
CHK2	-8.1	-9.6	NDR1	-4.5	-0.7	SLK	-1.4	-6.2
CK1 α	4	-10.9	NDR2	-0.2	-2	SRPK1	-3.1	-1.7
CK1 γ 1	-3.4	0.6	NEK1	-2.4	-10.6	SRPK2	-5.5	-1.5
CK1 γ 2	-0.4	2.7	NEK2	-4.4	-6.2	TAOK2	2	2.8
CK1 γ 3	-4.9	-1.2	NEK4	-1.2	-1	TBK1	2.8	3.4
CK1 δ	-1.8	1.3	NEK6	-2.7	-3.5	TNIK	3.2	9.6
CK1 ε	-3.6	-2.1	NEK7	-1.5	-4.5	TSSK1	-9.9	-11.5
CK2 α 1/β	-4.9	-2.3	NEK9	-1.9	-3.8	TSSK2	0.2	-4.2
CK2 α 2/β	-4.8	-6	NuaK1	-4.2	3.7	TSSK3	-9.1	-12.1
CLK1	11.1	0.7	NuaK2	-4.5	3.8	WNK1	0.9	1.8
CLK2	-12.3	-4.2	p38 β	-3.7	-1.6	WNK2	3.4	3.3
CLK3	-9.4	-3.8	p38 γ	-3.1	-3	WNK3	6.8	3.6

Table S2. List of antibodies.

Antibody	Clone	Application	Vendor
anti-mouse CD103	M290	FCM	BD
anti-mouse CD11c	HL3	FCM	BD
anti-mouse CD152 (CTLA-4)	UC10-4B9	FCM	eBioscience
anti-mouse CD16/32	93	FCM	BD
anti-mouse CD25	PC61	FCM	BD
anti-mouse CD28	37.51	Stimulation	BD
anti-mouse CD3ε	145-2C11	Stimulation	BD
anti-mouse CD4	RM4-5	FCM	BD
anti-mouse CD40	3/23	FCM	BD
anti-mouse CD62L	MEL-14	FCM	BD
anti-mouse CD8a	53-6.7	FCM	BD
anti-mouse CD80	16-10A1	FCM	eBioscience
anti-mouse CD86	PO3.1	FCM	eBioscience
anti-mouse GITR	DTA-1	FCM	BD
anti-mouse IFNγ	XMG1.2	FCM	BD
anti-mouse IL-17A	TC11-18H10.1	FCM	BD
anti-mouse IL-2	JES6-5H4	FCM	BD
anti-mouse IL-4	11B11	FCM	BD
anti-mouse KLRG1	2F1/KLRG1	FCM	BioLegend
anti-mouse MHC Class II (I-A/I-E)	M5/114.15.2	FCM	BioLegend
anti-mouse/human Helios	22F6	FCM	BioLegend
anti-mouse/human phospho-STAT5 (Y694)	SRBCZX	FCM	eBioscience
anti-mouse/human phospho-STAT5 (Y694)	polyclonal (9351)	WB	Cell signaling technology
anti-phospho STAT5b (S731)	polyclonal (ab52211)	WB	Abcam
anti-phospho STAT3 (pS727)	49/p-Stat3	FCM	BD
anti-mouse/rat FoxP3	FJK-16s	FCM	eBioscience
anti-mouse/rat Ki-67	SolA15	FCM	eBioscience
anti-neuropilin-1	polyclonal (BAF566)	FCM	R&D

anti-β-actin	polyclonal (4967)	WB	Cell signaling technology
anti-Cdk19	polyclonal (HPA007053)	WB	Sigma
anti-Cdk8	polyclonal (sc-1521)	WB	Santacruz
anti-Cdk8	polyclonal (4101)	WB	Cell signaling technology
anti-Cdk8	polyclonal (61481)	IP	Active motif
anti-CyclinC	polyclonal (2950)	WB	Abcam
anti-MED12	polyclonal (4529)	WB	Cell signaling technology
anti-GAPDH	6C5	WB	Santacruz
anti-DO11.10	KJ1-26	FCM	BD
anti-human CD25	M-A251	FCM	BD
anti-human CD4	RPA-T4	FCM	BD
anti-human CD45RA	HI100	FCM	BD
anti-human Foxp3	236A/E7	FCM	eBioscience
anti-human/mouse CD44	IM7	FCM	BD
anti-CD271 (LNGFR)	ME20.4-1.H4	FCM	Miltenyie
anti-human/mouse Cdk8	polyclonal (PA1-21780)	PLA, IF	Invitrogen
anti-human/mouseSTAT5	9C8B50	PLA, IF	Biolegend